

RESEARCH ARTICLE

3D collagen fibrillar microstructure guides pancreatic cancer cell phenotype and serves as a critical design parameter for phenotypic models of EMT

T. J. Puls¹, Xiaohong Tan¹, Catherine F. Whittington^{1,2}, Sherry L. Voytik-Harbin^{1,3*}

1 Weldon School of Biomedical Engineering, Purdue University, West Lafayette, Indiana, United States of America, **2** Department of Oncology, Eli Lilly and Company, Indianapolis, Indiana, United States of America, **3** Department of Basic Medical Sciences, Purdue University, West Lafayette, Indiana, United States of America

* harbins@purdue.edu



OPEN ACCESS

Citation: Puls TJ, Tan X, Whittington CF, Voytik-Harbin SL (2017) 3D collagen fibrillar microstructure guides pancreatic cancer cell phenotype and serves as a critical design parameter for phenotypic models of EMT. PLoS ONE 12(11): e0188870. <https://doi.org/10.1371/journal.pone.0188870>

Editor: Rajeev Samant, University of Alabama at Birmingham, UNITED STATES

Received: March 2, 2017

Accepted: November 14, 2017

Published: November 30, 2017

Copyright: © 2017 Puls et al. This is an open access article distributed under the terms of the [Creative Commons Attribution License](https://creativecommons.org/licenses/by/4.0/), which permits unrestricted use, distribution, and reproduction in any medium, provided the original author and source are credited.

Data Availability Statement: All relevant data are within the paper and its Supporting Information file.

Funding: This study was supported by a Birck Nanotechnology Graduate Research Fellowship (TJP), a Lilly Innovation Fellowship Award (CFW), and the Purdue University Office of the Executive Vice President for Research and Partnerships Incentive Grant Program (SLVH). Eli Lilly provided support in the form of salary for CFW and research

Abstract

Pancreatic cancer, one of the deadliest cancers, is characterized by high rates of metastasis and intense desmoplasia, both of which are associated with changes in fibrillar type I collagen composition and microstructure. Epithelial to mesenchymal transition (EMT), a critical step of metastasis, also involves a change in extracellular matrix (ECM) context as cells detach from basement membrane (BM) and engage interstitial matrix (IM). The objective of this work was to develop and apply an *in-vitro* three-dimensional (3D) tumor-ECM model to define how ECM composition and biophysical properties modulate pancreatic cancer EMT. Three established pancreatic ductal adenocarcinoma (PDAC) lines were embedded within 3D matrices prepared with type I collagen Oligomer (IM) at various fibril densities to control matrix stiffness or Oligomer and Matrigel combined at various ratios while maintaining constant matrix stiffness. Evaluation of cell morphology and protein expression at both the cellular- and population-levels revealed a spectrum of matrix-driven EMT phenotypes that were dependent on ECM composition and architecture as well as initial PDAC phenotype. In general, exposure to fibrillar IM was sufficient to drive EMT, with cells displaying spindle-shaped morphology and mesenchymal markers, and non-fibrillar BM promoted more epithelial behavior. When cultured within low density Oligomer, only a subpopulation of epithelial BxPC-3 cells displayed EMT while mesenchymal MiaPaCa-2 cells displayed more uniform spindle-shaped morphologies and mesenchymal marker expression. Interestingly, as IM fibril density increased, associated changes in spatial constraints and matrix stiffness resulted in all PDAC lines growing as tight clusters; however mesenchymal marker expression was maintained. Collectively, the comparison of these results to other *in-vitro* tumor models highlights the role of IM fibril microstructure in guiding EMT heterogeneity and showcases the potential of standardized 3D matrices such as Oligomer to serve as robust platforms for mechanistic study of metastasis and creation of predictive drug screening models.

supplies, but did not have any additional role in the study design, data collection or analysis. Because of this affiliation, CFW's mentors at Eli Lilly provided editorial review of the manuscript, and Eli Lilly gave internal approval for publication.

Competing interests: This study was supported in part by a Lilly Innovation Fellowship Award (CFW). Author Catherine F. Whittington was employed by Eli Lilly and Company. There are no patents, products in development or marketed products to declare. This does not alter our adherence to all the PLOS ONE policies on sharing data and materials.

Introduction

Pancreatic ductal adenocarcinoma (PDAC) is one of the deadliest cancers with an estimated 5-year survival rate of around 5% [1]. PDAC is characterized by an intense stromal reaction, known as desmoplasia, where overactive cancer associated fibroblasts deposit excessive extracellular matrix (ECM), the bulk of which is fibrillar type I collagen [2,3]. It is widely thought that this stromal remodeling and dysregulation of cell-ECM homeostasis serves to promote cancer progression, including metastasis and drug resistance [2,4]. However, recent evidence suggests that desmoplasia may paradoxically play an important protective role, where resulting changes in ECM composition and architecture restrict rather than promote tumor growth and invasion [5]. Clearly, tumor-stromal ECM interactions play a critical role in PDAC pathophysiology; however, advanced *in-vitro* and *in-vivo* models are needed to achieve a more complete mechanistic understanding [5–7]. This knowledge gap, which exists for not only PDAC, but most solid tumors, precludes development of novel targeted therapies as well as identification of better predictors of patient therapeutic response. Since patients generally die from metastatic disease and PDAC has such a high metastasis rate, better understanding of how stromal ECM guides tumor phenotype and behavior is paramount to improving clinical outcomes [8–10].

ECM associated with PDAC, as well as normal tissues, is represented by two distinct types, namely basement membrane (BM) and interstitial matrix (IM). BM, composed primarily of laminin, non-fibrillar type IV collagen, and heparan sulfate proteoglycan, forms a thin sheet-like structure which supports and polarizes epithelial cell layers, separating them from the underlying interstitial tissue compartment. In contrast, the predominant component of IM is fibrillar type I collagen, within which individual mesenchymal cells (e.g., fibroblasts) reside. It is noteworthy that a hallmark of tumor metastasis is epithelial to mesenchymal transition (EMT), where epithelial cancer cells lose polarity and cell-cell associations while gaining a more mesenchymal and invasive phenotype. Fig 1 highlights salient features of tumor EMT, drawing attention to the altered stromal ECM context encountered by tumor cells as they increasingly interact with surrounding IM [9]. This marked difference in ECM context is often overlooked in conventional EMT schematics where IM is often excluded and intracellular events are emphasized [9,11].

Although it is evident that EMT is marked by dynamic tumor cell-ECM interactions, where cells may engage both BM and IM components, many experimental *in-vitro* models lack rigorous definition of relevant ECM molecular and physical properties [12,13]. In fact, tumor EMT research has traditionally focused on soluble factor (e.g., TGF- β 1) induction and intercellular signaling cascades [14,15]. However, since recent work suggest that matrix composition and physical properties (e.g. microstructure and viscoelastic properties) are involved in driving EMT, ideal tumor models should recreate the 3D fibrillar IM microstructure and geometry of cell-cell and cell-matrix associations to support physiologically relevant cell phenotypes, as well as enable mechanistic study through matrix tunability [2,16,17]. Unfortunately, many models fail to replicate these critical features of 3D tumor-ECM interactions and give rise to contradictory results. For example, breast cancer cells cultured on-top of Matrigel- or type I collagen-coated polyacrylamide (PA) gels showed that increased PA concentration (stiffness) enhanced EMT [18,19], while breast cancer and glioblastoma spheroids embedded within 3D fibrillar type I collagen matrices showed decreased mesenchymal behavior and invasiveness with increased collagen concentration (stiffness) [20–22]. These examples showcase how different geometries of cell-matrix interactions and ECM microstructures can yield conflicting results. Clearly, the ability to recreate ECM architecture and physical properties experienced by cancer cells *in vivo* will contribute to a more complete understanding of EMT and invasion.

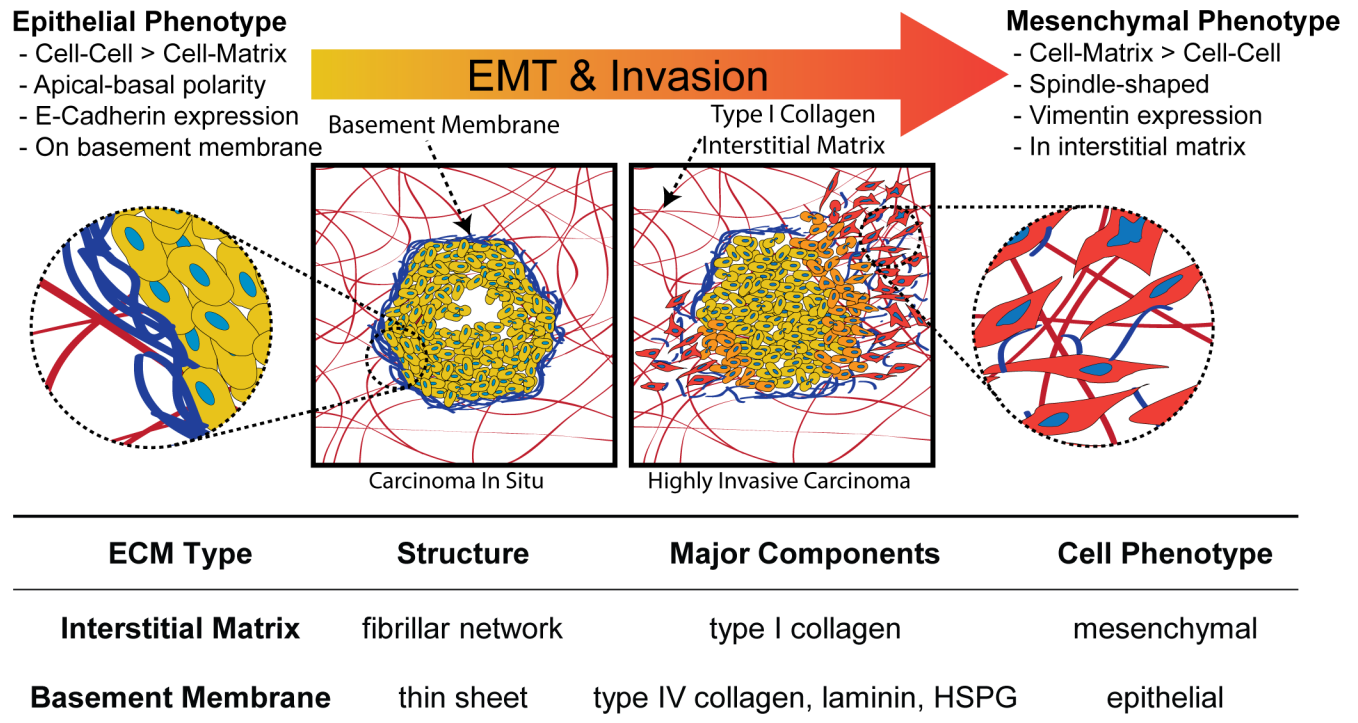


Fig 1. Overview of EMT and associated tumor stromal ECM interactions. Schematic shows key characteristics and progression of EMT, as epithelial cancer cells lose contact with basement membrane and interface with the surrounding interstitial matrix which is composed primarily of fibrillar type I collagen. Association with the stromal interstitial matrix correlates with transition from an epithelial to a mesenchymal phenotype. HSPG = heparan sulfate proteoglycan.

<https://doi.org/10.1371/journal.pone.0188870.g001>

Over the last several years, our laboratory has worked to develop new tools and methods for mechanistic study of fibrillar type I collagen self-assembly and the impact of resultant matrix physical properties on cell phenotype, function, and tissue morphogenesis. As part of this effort, we identified and standardized (ASTM F3089-14) a new soluble collagen subdomain (Oligomer) that retains natural, mature intermolecular crosslinks as well as the uncommon capacity for suprafibrillar self-assembly [23,24]. Oligomer displays rapid self-assembly (polymerization) *in vitro* and *in vivo*, forming highly-interconnected, D-banded collagen-fibril networks, which are similar to those found in tissues *in vivo*. This collagen formulation supports systematic modulation of the physical and biological properties of 3D IM microenvironments beyond what can be achieved with conventional collagen monomer formulations [23]. The tunable and robust matrices formed with Oligomer have proven useful in a variety of *in-vitro* applications including mesenchymal stem cell differentiation, vascular network formation, glioblastoma migration, and tissue engineering [22,25–27]. Type I oligomeric collagen (Oligomer) offers a promising alternative to materials traditionally used to mimic the IM in 3D cancer models.

The goal of the present work was to develop and apply an *in-vitro* 3D tumor-ECM model relevant to PDAC to further define the importance of ECM composition and physical properties in guiding EMT. Three well-characterized PDAC lines representing points along the EMT phenotypic spectrum were embedded within 3D self-assembled ECM microenvironments of defined composition and physical properties and changes in their phenotype evaluated. For this work, Oligomer was used to recreate the IM, and Matrigel, a reconstituted BM isolated from Engelbreth-Holm-Swarm (EHS) mouse sarcomas (a tumor rich in basement membrane)

[28] was used to mimic the BM. Matrigel is routinely used to approximate a BM-like environment since it provides a complex mixture of macromolecules including laminin, type IV collagen, and enactin. However, limitations associated with Matrigel include: 1) poorly defined molecular composition, 2) lot-to-lot variability (protein concentration and molecular composition), and 3) inability to recapitulate the specific nature of the biochemical and biophysical environment associated with all tumors (lacks type I collagen and *in-vivo* cross-linking) [28,29]. Overall, our results revealed a spectrum of matrix-driven phenotypes that were dependent on ECM composition, fibril architecture, and initial cell phenotype. In general, non-fibrillar BM (Matrigel) promoted epithelial behaviors such as clustered cell growth and E-cadherin expression. In low density Oligomer, the exposure to fibrillar IM promoted EMT of a subpopulation of epithelial BxPC-3 cells, while mesenchymal MiaPaca-2 cells more uniformly displayed mesenchymal characteristics. Interestingly, for all PDAC lines, increasing IM fibril density, which represents increasing desmoplasia, resulted in confined clustered growth due to the increased spatial constraints and matrix stiffness. Comparison of our results to those from other *in-vitro* models highlight the importance of ECM composition, microstructure, and mechanical properties in 3D *in-vitro* cancer models and establish Oligomer as a powerful tool in cancer research for mechanistic study of tumor-ECM interactions.

Materials and methods

Cell culture

BxPC-3, Panc-1, and MiaPaCa-2 cell lines were all obtained from American Type Culture Collection (ATCC, Manassas, VA) and maintained per manufacturer guidelines. BxPC-3 cells were grown in RPMI-1640 (Life Technologies, Grand Island, NY) and Panc-1 and MiaPaCa-2 cells were grown in high glucose DMEM (Hyclone, Logan, UT), all supplemented with 10% heat inactivated fetal bovine serum (HI FBS; Life Technologies), 100 U/mL penicillin, and 100 µg/mL streptomycin (Sigma Aldrich, St. Louis, MO). Growth medium of MiaPaCa-2 cells was additionally supplemented with 2.5% horse serum (Sigma Aldrich). Cells were maintained in a humidified environment of 5% CO₂ in air at 37°C, passaged at 70–80% confluency, and used in experiments at passage numbers between 6 and 14.

Creating *in-vitro* 3D tumor-ECM models

Type I oligomeric collagen was extracted from the dermis of market weight pigs (Beutler Meat Processing, Lafayette, IN) using acid solubilization as previously described [23]. Pig hides for this extraction process were obtained from a commercial meat-processing source according to Purdue University Animal Care and Use Committee (PACUC) guidelines, though specific approval was not needed. Extracted collagen was lyophilized for storage, dissolved in 0.01 N hydrochloric acid (HCl) for use, and standardized according to ASTM International Standard F3089-14 [30]. Briefly, Oligomer formulations were standardized based on molecular composition and polymerization capacity which is defined by the relationship between shear storage modulus (G' , Pa) of the polymerized matrix as a function of Oligomer concentration. Growth Factor Reduced Matrigel (Corning Life Sciences, Tewksbury, MA) was stored at -20°C and thawed at 4°C or on ice before use. Since Matrigel is known to have high batch-to-batch variability [28,31], all drug dosing experiments were performed with the same lot.

In-vitro 3D tumor-ECM models were created by encapsulating tumor cells within various reconstituted matrix compositions at 2×10^5 cells/mL. Matrigel was used undiluted, while Oligomer was diluted with 0.01 N HCl to desired concentrations and neutralized (pH = 7.4) with 10X phosphate-buffered saline (PBS) and 0.1 N sodium hydroxide as previously described [25]. To create matrices with different Oligomer:Matrigel ratios, neutralized Oligomer solution

(0.9 mg/mL) and Matrigel solutions were admixed at the following ratios—100:0, 75:25, 50:50, 25:75, 0:100 (volume:volume). To determine the effect of IM physical properties on EMT, Oligomer-only matrices were prepared at concentrations of 0.9, 1.5, 2.1 mg/mL which corresponded to shear storage modulus (matrix stiffness) values of approximately 100-, 500- and 1000 Pa. We have previously established that a positive correlation exists between Oligomer concentration, fibril density, and matrix stiffness [23,25,32]. 3D constructs were created by aliquoting matrix-cell suspensions (100 μ L, 2×10^5 cells/mL) into a 96 well plate followed by incubation at 37°C for 20–30 minutes to induce matrix polymerization or self-assembly. Immediately following self-assembly, the appropriate cell culture medium was added and constructs were cultured for four days with medium changes every other day.

Viscoelastic testing

Viscoelastic properties of matrices were determined using oscillatory shear mode on an AR2000 rheometer (TA Instruments, New Castle, DE) as previously described [23]. Samples were polymerized on the rheometer stage for 30 min followed by a shear-strain sweep from 0.1% to 4% strain at 1 Hz. The shear storage modulus (G') at 1% strain was used as a measure of matrix stiffness. Each sample was tested in triplicate ($n = 3$).

Staining and imaging

Tumor-ECM constructs were fixed in 3% paraformaldehyde (Mallinckrodt, Derbyshire, UK) and permeabilized using 0.1% Triton X-100 (Sigma Aldrich). To visualize cell morphology, F-actin was stained with Alexa Fluor 488 phalloidin (Life Technologies). For immunostaining, constructs were blocked with 1% bovine serum albumin (Jackson ImmunoResearch, West Grove, PA), followed by overnight incubation at 4°C with goat anti-rabbit primary antibodies for vimentin and E-cadherin (D21H3 and 24E10, Cell Signaling Technologies, Danvers, MA). After rinsing with 1X PBS, constructs were incubated overnight at 4°C with anti-rabbit conjugated Alexa Fluor 488 secondary antibody (A12379, Life Technologies) followed by nuclear counterstaining with Draq5 (Life Technologies).

Images were collected using laser scanning confocal microscopy on an Olympus IX81 inverted microscope with an Olympus Fluoview FV1000 system (Olympus, Tokyo, Japan). Image stacks of 150–200 μ m thickness with a 5 μ m step size were obtained using a 20X air or 60X water objective, and z-projections were created using Imaris software (Bitplane, Concord, MA). Confocal reflection microscopy was used to visualize the collagen-fibril microstructure [33].

Western blotting

Western blots were used to determine EMT protein expression on a population level for BxPC-3 and MiaPaca-2 in 2D and within constructs of varied Oligomer stiffness and Oligomer:Matrigel ratios. Cell lysates from 2D culture were obtained directly from cell culture flasks at 70–80% confluency using chilled 1X RIPA buffer (Millipore, Bedford, Massachusetts) containing 0.2% halt phosphatase and protease inhibitor cocktail (Thermo Fisher Scientific, Waltham, MA), and 2% phenylmethanesulfonyl fluoride solution (Sigma-Aldrich; 2%). Lysates from 3D culture were obtained by snap freezing constructs after four days of culture, grinding them into a powder, and dissolving in lysis buffer. All samples were kept on ice with periodic vortexing for one hour for 2D samples and three hours for 3D samples. Total protein concentration for all samples was determined using a BCA protein analysis kit (Pierce, Rockford, Illinois). Samples containing 30 μ g of protein were loaded onto a 4–20% Tris-HCl pre-cast gels (Bio-Rad, Hercules, CA) and transferred onto Trans-Blot Turbo Midi Nitrocellulose

membranes (Bio-Rad). After blocking in SEA BLOCK Blocking Buffer (Thermo Fisher Scientific) overnight at 4° C, the membranes were incubated with mouse antibodies against E-cadherin (Cell Signaling Technology, 1:1000), fibronectin (BD Biosciences, San Jose, CA; 1:1000), and vimentin (BD Biosciences; 1:1000) overnight at 4° C. Mouse antibody against glyceraldehyde 3-phosphate dehydrogenase (GAPDH; Meridian Life Science, Memphis, TN; 1:1000) was used as a loading control. Membranes were then washed in 1X PBS with 0.05% Tween-20 (Sigma-Aldrich) and incubated for two hours at room temperature with horseradish-peroxidase-conjugated IRDye 800CW anti-mouse secondary antibody (LI-COR Biosciences, Lincoln, NE; 1:10000). After multiple washes with the PBS/Tween solution, bands were visualized using Odyssey CLx Infrared Imaging System (LI-COR).

Determining gemcitabine sensitivity

PDAC cell sensitivity to gemcitabine (Santa Cruz Biotechnology, Dallas, TX) was determined by dosing with a 10-point drug dilution (1:5 dilution starting at 200 μ M) and calculating IC50 values from data obtained with Alamar Blue metabolic indicator (Invitrogen, Frederick, MD). Cells were seeded in 96-well plates either on 2D tissue culture plastic at 4×10^3 cells/well or within different 3D matrix formulations at 2×10^5 cells/mL (100 μ L or 2×10^4 cells/well). After 24 hours, culture medium was replaced with medium containing gemcitabine dilutions, 20 μ M staurosporine (positive kill control; Santa Cruz Biotechnology), or 1% DMSO (negative control; Sigma Aldrich). Treatments were replenished after 48 hours. Each treatment was performed in triplicate, and all experiments were repeated at least 3 times ($N \geq 3$; $n = 3$).

After 72 hours of treatment, fresh medium containing 10% Alamar Blue solution and 1% FBS was added to each well, and well-plates were incubated for an additional 8 hours. Fluorescence intensity of medium was measured spectrofluorometrically using 530 nm/590 nm excitation/emission on a SpectraMax M5 Microplate Reader (Molecular Devices, Sunnyvale, CA). Raw intensity values were normalized to the positive and negative controls with the following equation: % Cell Viability = $(I_n - I_{STS}) / (I_{DMSO} - I_{STS}) \times 100\%$. I_n represents the intensity value of the n th dilution. I_{STS} and I_{DMSO} represent intensities recorded from positive kill control and negative control, respectively. GraphPad Prism (GraphPad Software Inc., San Diego, CA) was used to fit a four-parameter logistic curve. The automatic robust outlier detection algorithm within Prism was used to detect and exclude outliers from the final fit. Reported values represent relative IC50, defined as the halfway point between the bottom and top plateaus of each curve.

S-phase fraction determination

Total cell number and the fraction of cells undergoing S-phase were determined using Click-iT Edu (Life Technologies) followed by quantitative image analysis using Imaris (Bitplane). Briefly, after 3 days of culture, tumor-ECM construct medium was refreshed with medium containing 10 μ M 5-ethynyl-2'-deoxyuridine (Edu) and cultured for another 24 hours. Constructs were then fixed with 3% paraformaldehyde (Mallinckrodt), permeabilized using 0.1% Triton X-100 (Sigma Aldrich), and incubated with Click-iT reaction cocktail prepared following manufacturer's instructions. Constructs were subsequently counterstained with Draq5 and z-stack images of 50 μ m thickness were collected using laser scanning confocal microscopy on an Olympus IX81 inverted microscope with an Olympus Fluoview FV1000 system (Olympus) and a 20X air objective. The Imaris spot detection algorithm was used to independently detect nuclei stained with Click-iT Edu and Draq5 for quantification of the number of cells undergoing S-phase and total cell number, respectively. S-phase fraction was then calculated by dividing the number of S-phase cells by the total number of cells. Images (2 per well) from two

separate experiments ($N = 2$) performed in triplicate ($n = 3$) for each matrix stiffness were used for final calculations and statistics.

Statistical analysis

Statistical analyses were performed using SAS (Statistical Analysis System; SAS Institute Inc., Cary, NC). For gemcitabine sensitivity, a two-factor ANOVA was used to compare stromal ECM microenvironment and cell type. Main effects were compared using Tukey-corrected pairwise comparisons for one factor while holding the other factor constant. A one-factor ANOVA with Tukey-corrected pairwise comparisons was used to analyze viscoelastic testing data. S-phase fraction data was analyzed with a three-factor ANOVA which included experiment number and replicate as factors in order to test their significance and not falsely inflate the degrees of freedom in the model. In all cases, differences were considered statistically significant when $p < 0.05$.

Results

Established PDAC lines cultured in 2D represent phenotypes along the EMT spectrum

Throughout this work, three established PDAC lines with distinct EMT phenotypes were used (BxPC-3 –epithelial, Panc-1 –intermediate, and MiaPaCa-2 –mesenchymal) to evaluate ECM-guided EMT. Literature based characteristics of these PDAC lines are summarized in [Fig 2A](#). To validate each cell line's initial phenotype, cell morphology and expression patterns of EMT marker proteins, E-cadherin and vimentin [8,34], were determined following 2D culture. Here, we defined epithelial phenotype as cells growing in tight clusters with prominent E-cadherin expression, high cell-cell interactions, and primarily cortical actin [35]. On the other hand, mesenchymal phenotype was characterized by individual cells with spindle-shaped morphology, prominent actin projections, high cell-ECM interactions, and pronounced vimentin expression [35].

Consistent with previously published work [37,38], BxPC-3 cells displayed an epithelial phenotype in 2D culture, growing as cell clusters with prominent E-cadherin expression, while MiaPaCa-2 cells were mesenchymal, displaying the typical spindle-morphology with vimentin expression ([Fig 2B](#)). Panc-1 cells exhibited an intermediate phenotype, growing as clusters with some actin projections and expressing vimentin but not E-cadherin ([Fig 2B](#)). In addition to phenotype, gemcitabine sensitivity was measured with relative IC50 values calculated from 10-point dose response curves, showing that in 2D, Panc-1 cells were the most resistant to gemcitabine, followed by BxPC-3, and then MiaPaCa-2 ([Fig 2C](#)). These results were consistent with previously published studies where similar experimental conditions and assay methods were employed ([S1 Table](#)).

At matched stiffness, Oligomer induces EMT and Matrigel induces MET

The effect of various ECM ligands and soluble factors on tumor cell plasticity and EMT phenotype is routinely studied for cells cultured on 2D surfaces [39–42]. However, less is known regarding how cells sense and respond to 3D IM and BM environments with defined biochemical and biophysical attributes [21,43,44]. Here, PDAC lines were cultured within 3D type I collagen-fibril matrices prepared with Oligomer and tumor BM-like microenvironments prepared with Matrigel. Since Oligomer and Matrigel represent different ECM compositions and microstructures, an Oligomer concentration was chosen to yield matrix stiffness values that

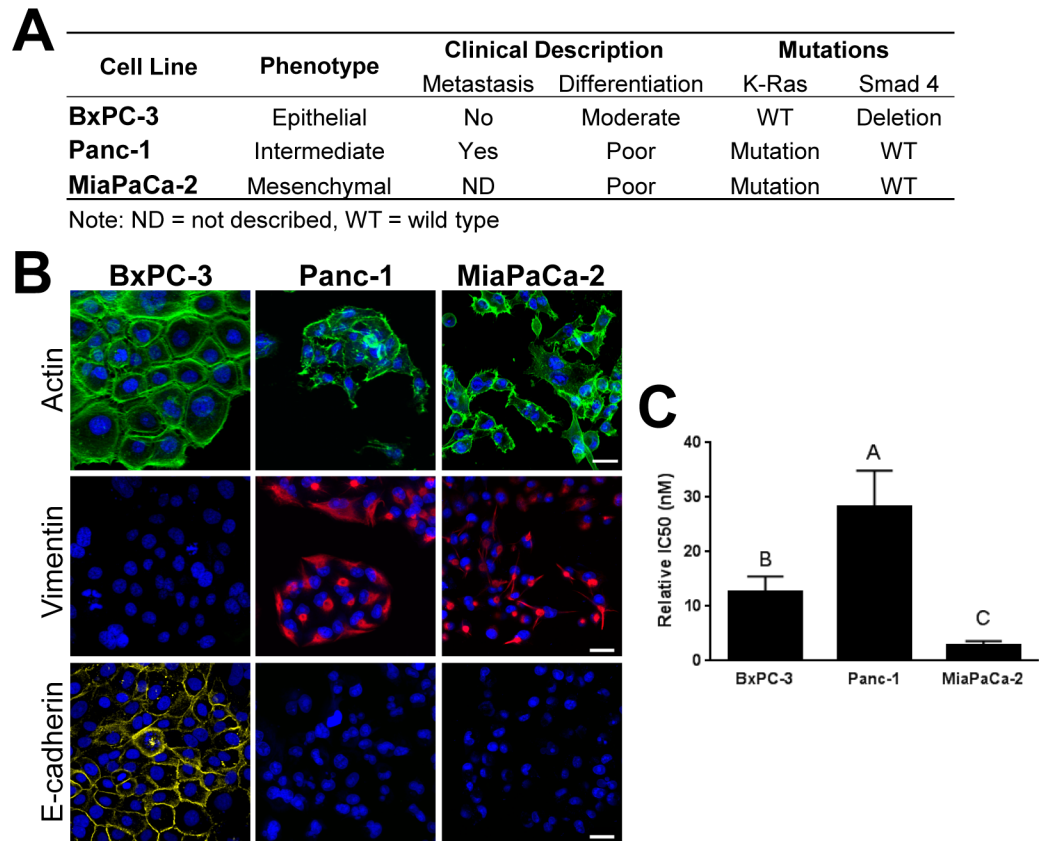


Fig 2. PDAC lines differ in EMT phenotype and gemcitabine resistance when cultured on 2D plastic. (A) Table summarizing pancreatic cell line phenotype, patient derivation, and relevant mutations [36]. (B) BxPC-3, Panc-1, and MiaPaCa-2 cells were cultured on 2D plastic (4×10^3 cells/well) for 4 days, stained for actin (green), vimentin (red), E-cadherin (yellow), and nuclei (blue), and imaged using confocal microscopy. Images represent z-stack projections (20 μ m thickness; scale bar = 30 μ m). (C) Gemcitabine IC50 values (mean \pm SD) were determined from 10-point dose response curves for cell lines cultured on 2D plastic. Letters indicate statistically different groups ($p < 0.05$, $n = 5$).

<https://doi.org/10.1371/journal.pone.0188870.g002>

matched undiluted Matrigel ($G' = 100$ Pa), avoiding stiffness as a possible confounding variable.

As summarized in Fig 3, the fibrillar type I collagen matrices formed by Oligomer (100 Pa) promoted various degrees of EMT and mesenchymal behavior, while Matrigel induced more MET and epithelial behavior. More specifically, when grown within Oligomer (100 Pa), all PDAC lines showed decreased cell-cell associations and more pronounced spindle-shaped morphology with prominent actin projections. A subset of BxPC-3 cells shifted to expressing both vimentin and E-cadherin in Oligomer as detected by immunostaining, while both Panc-1 and MiaPaCa-2 cells only expressed vimentin. In contrast, all PDAC lines cultured within Matrigel grew as tight clusters with high nuclear to cytoplasmic ratios and cortical actin (Fig 3). Additionally, within Matrigel, Panc-1 cells shifted to expressing both E-cadherin and vimentin, while BxPC-3 and MiaPaCa-2 cells expressed E-cadherin only and vimentin only, respectively. Collectively, these results document that specific ECM ligands, and their associated microstructures, are critical determinants of PDAC phenotype and behavior, especially as it relates to EMT and MET.

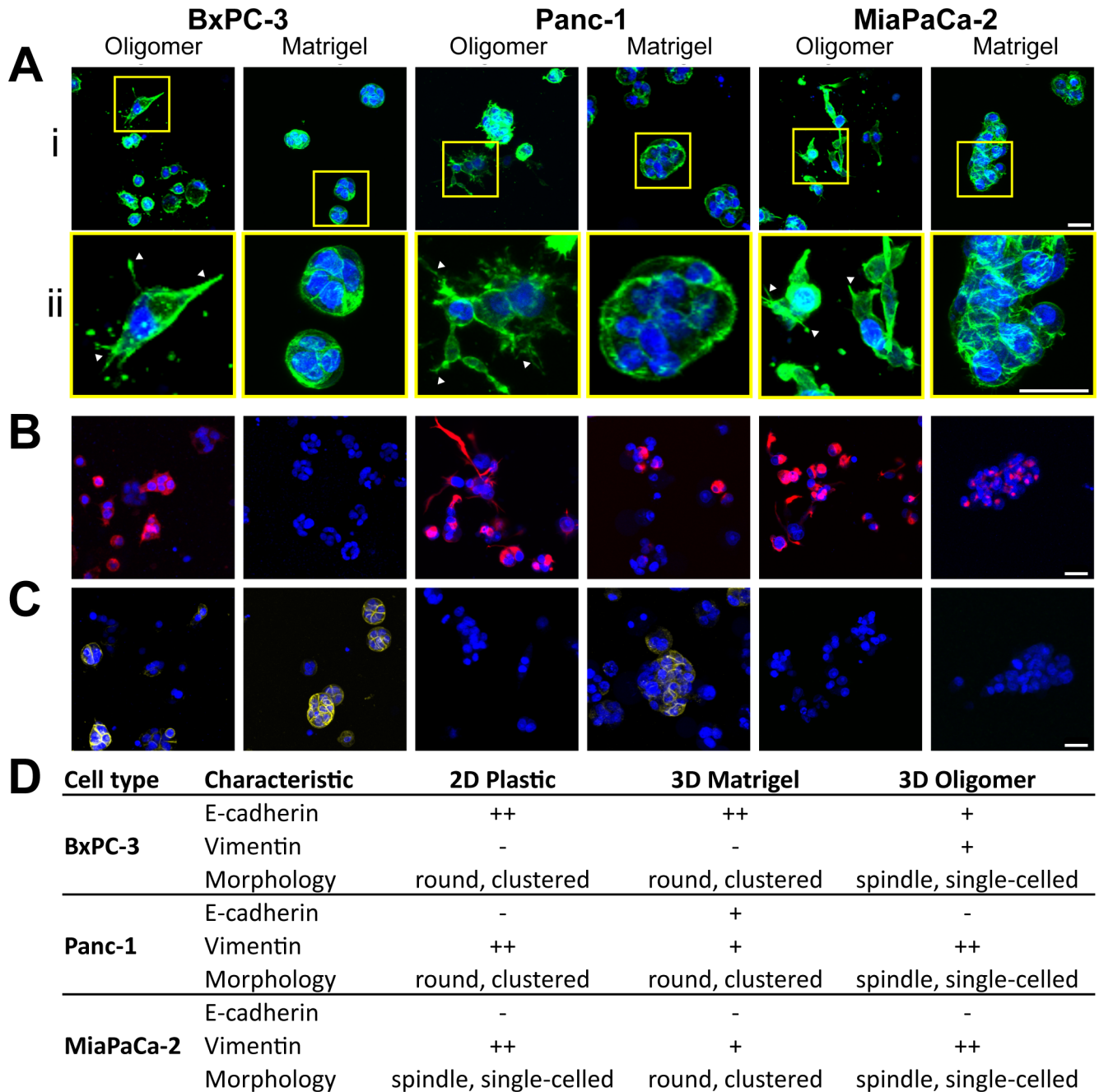


Fig 3. Stromal ECM drives pancreatic cancer cell morphology and phenotype. BxPC-3, Panc-1, and MiaPaCa-2 cells were cultured (2×10^5 cells/mL) for 4 days within Oligomer (0.9 mg/mL; 100 Pa) and Matrigel (100 Pa). Constructs were stained for actin (A; green), vimentin (B; red), E-cadherin (C; yellow), and nuclei (blue) and imaged using confocal microscopy. Images represent z-stack projections (100 μ m thickness; scale bar = 30 μ m). Yellow boxes represent 3X digitally zoomed sections (ii) and arrowheads note prominent actin protrusions. (D) Table summarizing protein expression and morphological observations from panels A-C.

<https://doi.org/10.1371/journal.pone.0188870.g003>

Dose response analysis reveals matrix-dependent gemcitabine sensitivity of PDAC lines

In high throughput 2D drug screening, IC50 is commonly used as a measure of drug sensitivity. However, fewer studies report IC50 values for 3D culture models because adapting drug

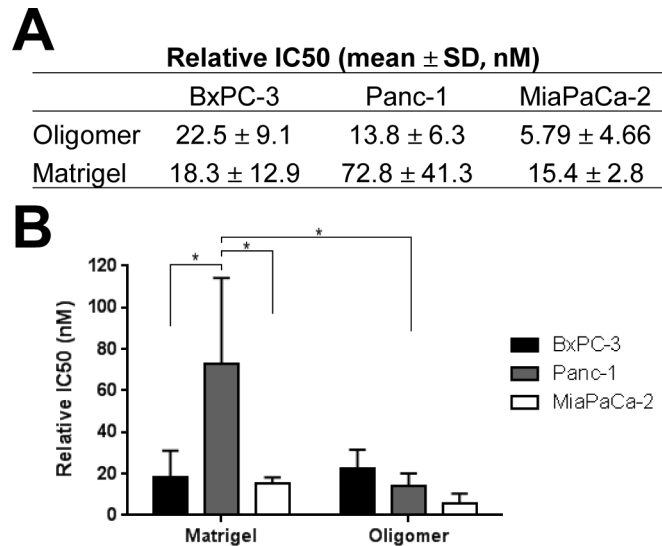


Fig 4. Sensitivity of PDAC lines to gemcitabine depends on 3D matrix type. (A) Table and (B) graph summarizing gemcitabine IC50 values (mean ± SD) for PDAC lines cultured (2×10^5 cells/mL) for 4 days within Oligomer (0.9 mg/mL, 100 Pa) or Matrigel (100 Pa). Asterisk (*) indicates statistically different groups ($p < 0.05$, $N = 3-4$, $n = 3$).

<https://doi.org/10.1371/journal.pone.0188870.g004>

dosing protocols and analyses to 3D formats tends to be more difficult, time consuming, and resource intensive [45,46]. To demonstrate that our 3D tumor-ECM model is amenable to medium and high throughput drug screening, the relative IC50 values of gemcitabine were determined for each PDAC line within 3D Oligomer and Matrigel, prepared with matched matrix stiffness. As shown in Fig 4, gemcitabine sensitivity of PDAC lines was matrix dependent. When cultured within Oligomer (100 Pa), PDAC lines showed statistically similar ($p > 0.05$) IC50 values, ranging from about 6 to 23 nM. In contrast, when cultured within Matrigel, Panc-1 cells displayed a significantly ($p < 0.05$) higher IC50 value of 72.8 ± 41.3 nM compared to BxPC-3 and MiaPaCa-2 cells which measured 18.3 ± 12.9 nM and 15.4 ± 2.8 nM, respectively. Further, IC50 values for BxPC-3 and MiaPaCa-2 cells in Matrigel were statistically similar ($p > 0.05$) to those obtained for Oligomer (100 Pa), while Panc-1 cells' IC50 was significantly lower ($p < 0.05$) in Oligomer compared to Matrigel. It is worth noting that Panc-1 cells showed greater resistance to gemcitabine compared to the other PDAC lines when cultured within Matrigel (Fig 4) and on plastic (Fig 2C), but not within Oligomer. Collectively, these results emphasize that the tumor microenvironment, including ECM composition and microstructure, is a critical determinant of PDAC drug sensitivity.

Varying stromal IM to BM ratio guides PDAC phenotype and EMT

As tumor cells become exposed to fibrillar type I collagen, whether deposited by stromal cells or encountered at the tumor-tissue interface, cells may simultaneously interact with both IM and BM components, thus engaging different integrin receptors [47,48]. To define how such dynamic cell-ECM signaling affects PDAC phenotype and EMT, PDAC cells were cultured within matrices prepared with different ratios of Oligomer and Matrigel, representing IM and BM, respectively. These experiments were conducted with only two PDAC lines, BxPC-3 and MiaPaCa-2, representing epithelial and mesenchymal phenotypes.

Matrix microstructure and stiffness were defined to determine how varying Oligomer:Matrigel (IM:BM) ratio altered matrix self-assembly and physical properties (Fig 5). As

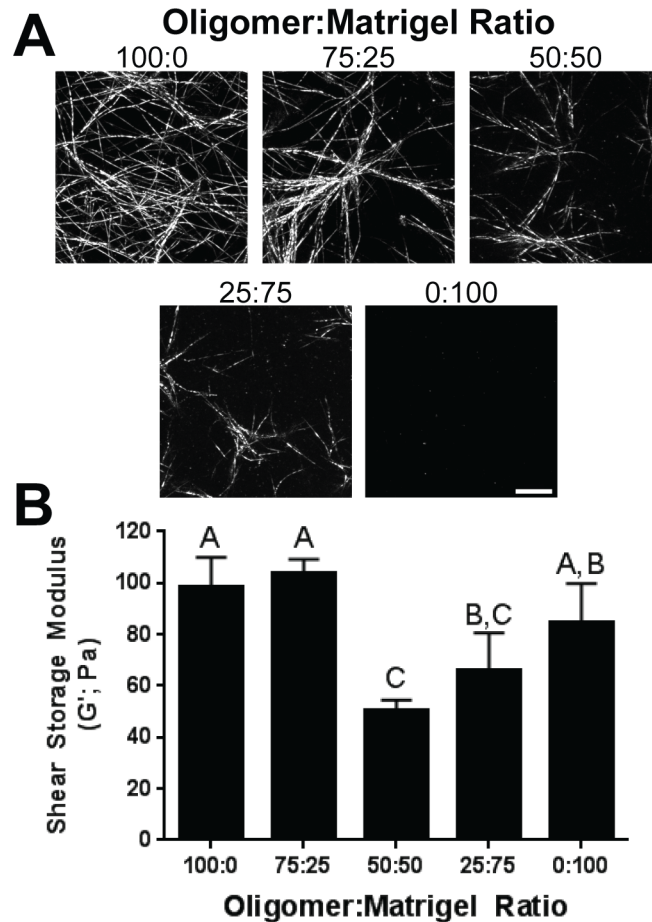


Fig 5. Oligomer:Matrigel ratio affects matrix microstructure and stiffness. (A) Images represent z-stack projections (10 μ m thickness; scale bar = 10 μ m) from confocal reflection microscopy of matrices prepared with varying Oligomer:Matrigel ratios. (B) Matrix stiffness values are given as shear storage modulus (G'; mean \pm SD). Letters indicate statistically different groups ($p < 0.05$, $n = 3$).

<https://doi.org/10.1371/journal.pone.0188870.g005>

visualized by confocal reflectance microscopy, matrix architecture varied from the highly-branched fibrillar network for Oligomer (100:0) to no visible fibril microstructure in Matrigel (0:100), emphasizing differences in self-assembly capacity and matrix physical properties. Fibril density and length appeared to decrease with decreasing Oligomer:Matrigel ratio with 100:0 and 75:25 displaying dense branched fibril networks and 50:50 and 25:75 exhibiting fewer and shorter fibrils. Observed differences in microstructure were consistent with measured alterations in matrix mechanical properties. More specifically, matrix stiffness (G') values for 100:0 and 75:25 were statistically similar ($p > 0.05$) while 50:50 and 25:75 were significantly softer ($p < 0.05$). As expected for this experiment, 0:100 (Matrigel) and 100:0 (Oligomer) stiffness values were statistically similar ($p > 0.05$), since Oligomer concentration was chosen to match the stiffness of undiluted Matrigel.

Analysis of PDAC cell morphology and protein expression as a function of Oligomer:Matrigel ratio further supported the supposition that Oligomer induced EMT and Matrigel induced MET to an extent that was dependent upon initial PDAC cell phenotype. As the Oligomer:Matrigel ratio increased, an increased number of BxPC-3 cells transitioned from an epithelial morphology to smaller cell clusters or individual cells displaying prominent cytoplasmic projections (Fig 6A). In addition, these subpopulations showed an apparent increase in vimentin

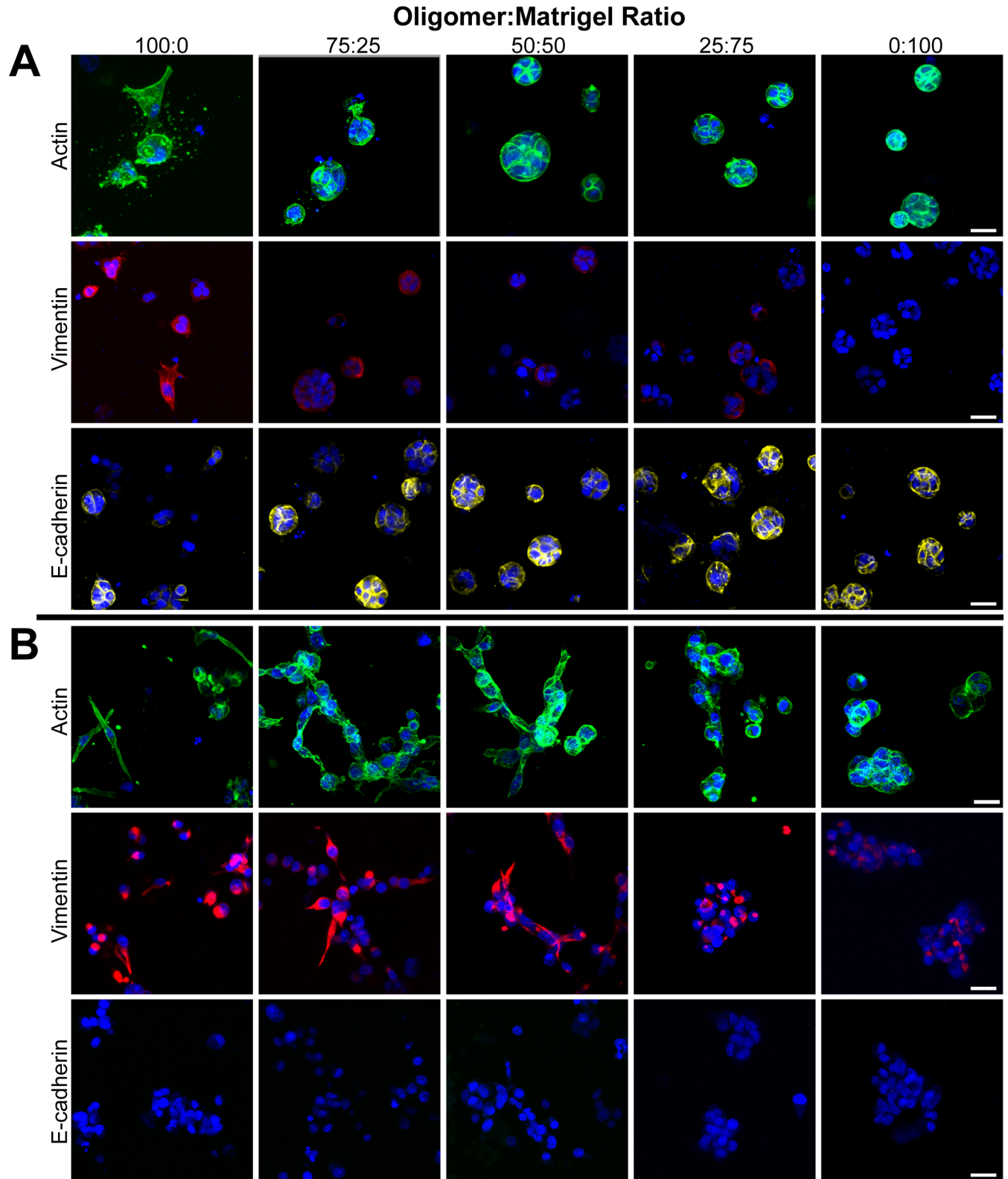


Fig 6. Oligomer:Matrigel ratio modulates EMT phenotype. (A) BxPC-3 and (B) MiaPaCa-2 cells were cultured (2×10^5 cells/mL) within 3D matrices prepared with various Oligomer:Matrigel ratios for 4 days. Constructs were stained for actin (green), vimentin (red), E-cadherin (yellow), and nuclei (blue) and imaged using confocal microscopy. Images represent z-stack projections (100 μ m thickness; scale bar = 30 μ m).

<https://doi.org/10.1371/journal.pone.0188870.g006>

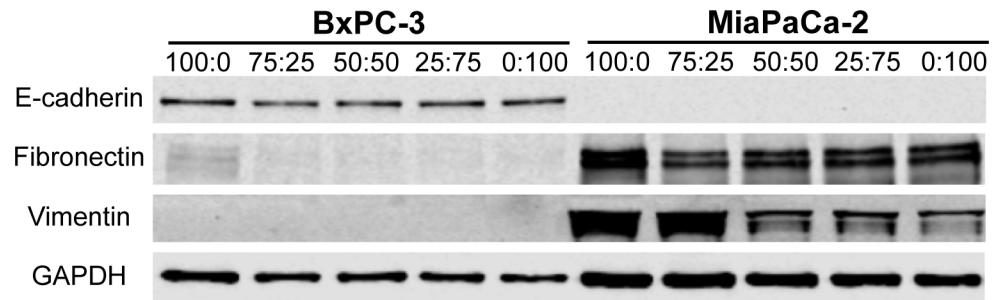


Fig 7. Oligomer:Matrigel ratio effects on population level EMT protein expression is dependent upon initial PDAC phenotype. Western blots showing EMT protein expression for BxPC-3 and MiaPaCa-2 (2×10^5 cells/mL) cultured for 4 days within 3D matrices prepared at various Oligomer:Matrigel ratios.

<https://doi.org/10.1371/journal.pone.0188870.g007>

expression and decreased E-cadherin expression as the Oligomer:Matrigel ratio increased. Interesting these differences in marker protein expression were not observed when measured at a population level via western blots which showed no change in E-cadherin expression and no detectable vimentin expression with changing ratios (Fig 7). Modest fibronectin expression was observed in BxPC-3 cells cultured in 100:0, but expression decreased to undetectable levels once Matrigel was introduced into the construct.

MiaPaCa-2 cells, on the other hand, showed more drastic changes in morphology (Fig 6B) and population-level protein expression (Fig 7) with varying Oligomer:Matrigel ratio, while immunostaining revealed only modest changes in EMT protein expression patterns (Fig 6B). Within the lowest Oligomer:Matrigel ratios (0:100 and 25:75), MiaPaCa-2 cells were tightly packed with little to no actin projections. As Oligomer content increased, cells became progressively more singular and spindle-shaped, with cells in 75:25 aligning into networks resembling the invasive front of a tumor. Immunostained MiaPaCa-2 cells did not express detectable E-cadherin in any matrix composition. While vimentin expression was observed in all matrices, it appeared to be reduced within 0:100 and 25:75 and shifted from uniformly distributed throughout the cytoplasm to localized around cell nuclei. Analysis by western blot confirmed immunostaining results with Oligomer:Matrigel ratio showing having no effect on MiaPaCa-2 E-cadherin expression and vimentin expression decreasing with Matrigel content (Fig 7). A similar decreasing expression trend was observed for fibronectin with highest expression levels occurring in MiaPaCa-2 cells cultured within 100:0. Altogether, these results suggest that i) a combination of IM and BM interactions plays an important role in guiding tumor cell plasticity and EMT, and ii) ECM type and microstructure differentially regulate cell phenotype depending on the cells' initial EMT status.

Increasing collagen-fibril density (matrix stiffness) controls mesenchymal behavior and suggests matrix dependent correlation between S-phase fraction and drug sensitivity

Pancreatic cancer is known for significant desmoplasia, characterized by over-active stellate cells and fibroblasts which increase fibrillar type I collagen deposition [3,49]. However, the precise role played by desmoplasia and type I collagen in tumor-stromal ECM interactions and tumor progression remains uncertain [5,50,51]. In order to better define the role of IM physical properties in regulating EMT and drug sensitivity, matrix stiffness was varied by altering the Oligomer concentration or fibril density as seen in Fig 8A and 8B. The positive correlation between oligomer concentration, fibril density, and matrix stiffness has been established

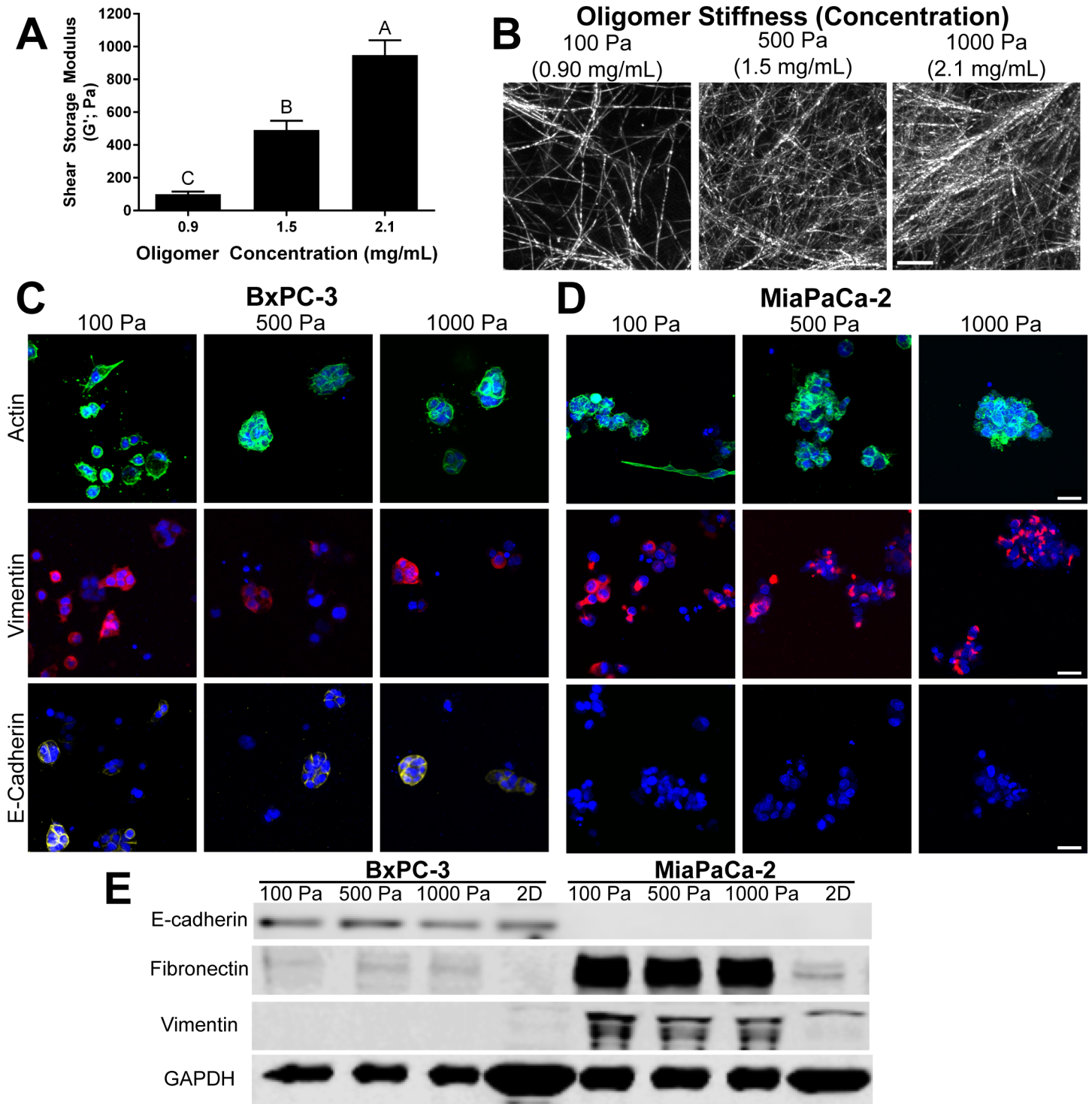


Fig 8. Stromal interstitial matrix stiffness alters PDAC cell phenotype. (A) Matrix stiffness values of matrices prepared at Oligomer concentrations of 0.9, 1.5, 2.1 mg/mL are given as shear storage modulus (G' ; mean \pm SD) with letters indicating statistically different groups ($p < 0.05$, $n = 3$). (B) Images represent z-stack projections of confocal reflection microscopy ($10 \mu\text{m}$ thickness, scale bar = $10 \mu\text{m}$) of matrices (C) BxPC-3 and (D) MiaPaCa-2 cells were cultured (2×10^5 cells/mL) within these three matrices for 4 days. Constructs were stained for actin (green), vimentin (red), E-cadherin (yellow), and nuclei (blue) and imaged using confocal microscopy. Images represent z-stack projections ($100 \mu\text{m}$ thickness; scale bar = $30 \mu\text{m}$). (E) Western blot measurement of EMT protein expression for BxPC-3 and MiaPaCa-2 cultured for 4 days within various Oligomer matrices and on 2D tissue culture plastic.

<https://doi.org/10.1371/journal.pone.0188870.g008>

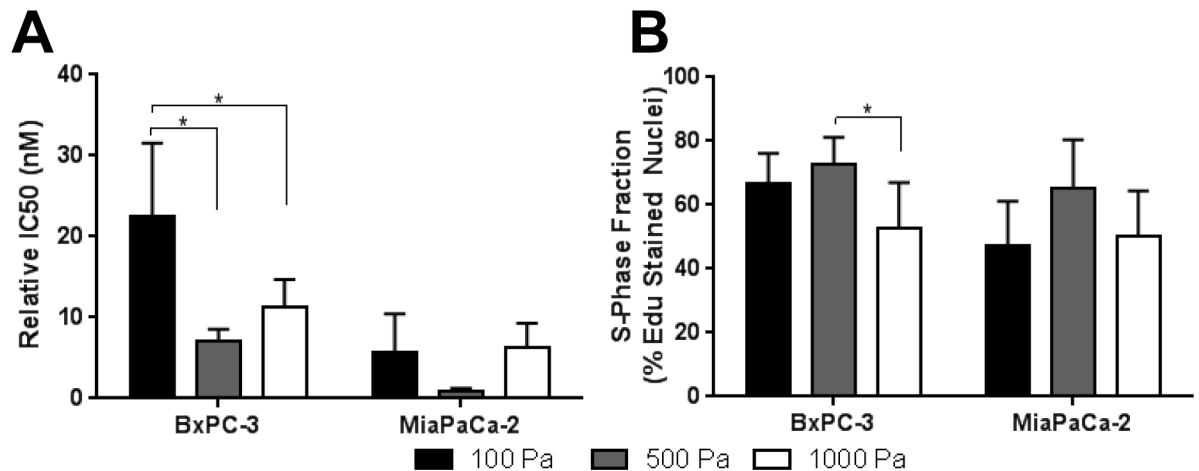


Fig 9. Stromal interstitial matrix stiffness alters PDAC cell gemcitabine sensitivity and proliferative capacity. (A) Gemcitabine IC50 values (mean \pm SD; n = 3) and (B) S-phase fraction (mean \pm SD; N = 2, n = 3) for BxPC-3 and MiaPaCa-2 cells cultured for 4 days within 3D Oligomer (2×10^5 cells/mL) prepared at stiffness values of 100 Pa (0.9 mg/mL), 500 Pa (2 mg/mL), and 1000 Pa (3 mg/mL). Asterisk (*) indicates statistically different groups ($p < 0.05$); note that values between different cell types were not compared.

<https://doi.org/10.1371/journal.pone.0188870.g009>

previously [23,25,32]. PDAC lines were cultured within Oligomer matrices prepared with stiffness values of 100, 500, and 1000 Pa and analyzed for changes in phenotype, S-phase fraction, and gemcitabine sensitivity. The S-phase fraction was quantified since gemcitabine causes checkpoint arrest and cell death by incorporating into DNA during S-phase [52].

When cultured in low stiffness (100 Pa) Oligomer, a significant subpopulation of BxPC-3 and nearly all MiaPaCa-2 cells took on a spindle-shaped, mesenchymal morphology. However, as Oligomer density and stiffness increased, both cell types grew as clustered aggregates, displaying more epithelial-like behavior (Fig 8C and 8D). Western blot data showed no appreciable changes in EMT marker protein expression as a function of Oligomer stiffness (Fig 8C–8E). BxPC-3 expressed E-cadherin in the majority of cells in immunostained samples and also showed prominent bands for E-cadherin. On the other hand, while immunostaining showed vimentin expression in some BxPC-3 cells, expression was not detectable in western blots. Conversely, MiaPaCa-2 showed vimentin expression with no E-cadherin expression in all conditions in both immunostaining and western blots. Both lines showed fibronectin expression under each condition, though bands for BxPC-3 were very faint. Compared to cells cultured on 2D, Oligomer appeared to promote fibronectin expression in BxPC-3 and both fibronectin and vimentin expression in MiaPaCa-2 (Fig 8E). It is noteworthy that this upregulation was observed even though GAPDH (loading control) for 2D samples appeared heavier, despite efforts to load equal protein amounts for all samples. The heavier banding for 2D samples is likely due to some residual matrix protein in 3D samples, which would effectively decrease the ratio of cellular protein to total protein for 3D samples compared to 2D samples.

Finally, gemcitabine sensitivity and S-phase fraction were measured for BxPC-3 and MiaPaCa-2 cells within Oligomer of varied stiffness. Only IC50 values for BxPC-3 in 100 Pa were statistically ($p < 0.05$) different from 500 Pa and 1000 Pa; however, both lines showed apparent inverted bell-shaped relationships with minima at 500 Pa (Fig 9A). Interestingly, these minima in gemcitabine sensitivity appeared to correlate with maxima in S-phase fraction, also at 500 Pa, albeit with no statistical significance (Fig 9B). Overall, these results show that matrix stiffness, altered through changing fibril density, can be a regulating factor in not only EMT, but also cell cycle progression and drug sensitivity.

Discussion

In-vitro tumor models provide important basic research and drug screening tools; however, few adequately recreate metastasis and associated EMT, which remains the major cause of PDAC and other cancer-related deaths. The present work focused on 3D tumor-ECM model development, emphasizing the need for more accurate recapitulation of the PDAC desmoplastic ECM composition and microstructure, which is typically characterized by high levels of fibrillar type I collagen [53]. This fibrous, stiff ECM microenvironment is generally thought to compromise drug transport, decrease tumor chemosensitivity, and enhance EMT and tumor invasion [4,6,54]. However, our 3D tumor-ECM model revealed that PDAC phenotype and behavior vary significantly with initial tumor cell phenotype and depend largely on both the biochemical and biophysical properties of the surrounding stromal ECM. Although fibrillar type I collagen was found to generally promote enhanced expression of specific mesenchymal marker proteins, PDAC morphology as well as the extent of cell-ECM interactions and phenotypic heterogeneity were largely determined by matrix biophysical properties, namely fibril density and associated matrix stiffness. Such results are consistent with recent *in-vivo* preclinical studies that have shown dense type I collagen-fibril architectures restrain rather than promote PDAC EMT and metastasis [55,56].

The PDAC stromal ECM is comprised of BM and IM—two ECM types that differ substantially in their molecular composition, microstructure, and viscoelastic properties [57,58]. BM provides a thin, mechanically weak barrier that separates epithelium (e.g., glands, ducts) and endothelium (e.g., blood vessels, lymph vessels) from underlying interstitial tissues. It is primarily composed of type IV collagen which forms highly intertwined supramolecular networks with laminin, entactin, nidogen, and other molecules [59]. In contrast, IM is primarily composed of type I collagen which exhibits hierarchical self-assembly to form the D-banded fibrillar architecture of interstitial connective tissues. During IM synthesis and fibril self-assembly, intermolecular cross-links form between collagen molecules by an enzyme-mediated process, imparting significant stability and strength to the fibrillar matrix [60]. These two ECM types are of particular interest to PDAC because poor patient prognosis has been correlated with a decrease in BM proteins and a corresponding increase in IM content [53,61].

In the present work, Matrigel was used to approximate the BM, and Oligomer was used to recreate and tune the fibrillar IM microenvironment. While no research tools exist today that allow accurate BM recreation *in vitro*, Matrigel, a murine tumor BM extract, has been used extensively to mimic the BM in 3D cancer models. Although Matrigel as a natural hydrogel formulation contains many BM components, it does not exhibit the molecular cross-linking or architecture found in BM *in vivo* and shows significant lot-to-lot variability and low mechanical properties [57,62]. Oligomer, on the other hand, is a soluble type I collagen subdomain that, unlike conventional monomer formulations (atelocollagen and telocollagen), retains mature intermolecular cross-links formed *in vivo* [25]. As a result, this formulation exhibits high-order supramolecular assembly, giving rise to highly branched fibril networks with significantly improved physiological relevance, mechanical integrity, and resistance to proteolytic degradation [23,24,32,63]. Because Oligomer is standardized based upon its self-assembly or fibril-forming capacity, it supports tunability over a broad range of fibril microstructures and matrix stiffness values and shows excellent reproducibility within and between laboratories [23,32]. The distinct self-assembly capacity of Oligomer has been documented in previous published work, where polymerization of Oligomer over the concentration range of 0.5–4 mg/mL yields matrices with G' values of 40–1500 Pa while matrices prepared with telocollagen and atelocollagen, formulations commonly used in other studies, cover G' ranges of 2–300 Pa and 2–50 Pa, respectively [23]. The use of Oligomer in the present work allowed PDAC cells to


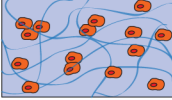

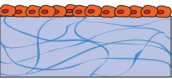

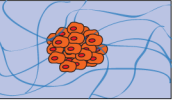
engage type I collagen IM in a natural fibrillar context with systematic control of fibril density and associated matrix stiffness.

Fig 10 summarizes various *in-vitro* tumor models used for EMT and invasion studies, highlighting culture format, ECM scaffold material, and ECM biophysical properties as critical design parameters for recreating pathophysiologically relevant cell-matrix interactions *in vitro* [17,64]. Based on this review, the majority of EMT and invasion studies performed to date have focused on breast cancer, underscoring a need for more pancreatic cancer investigations. Most work targeting ECM-guided EMT has been performed using cell monolayers grown on either 2D plastic surfaces with adsorbed matrix proteins or on-top of 3D substrates (also known as semi-3D). On the other hand, studies focused on tumor invasion, a hallmark of metastasis, involve embedding multi-cellular spheroids or organoids within 3D matrices prepared from monomeric type I collagen. Although not addressed specifically in the table, this review also revealed that culture format often dictates whether cellular or population level analyses are used and that 3D embedment experiments often lack population level evaluations [65–67]. Finally, only one other tumor EMT study was identified that involved 3D embedment of single cells within a fibrillar type I collagen matrix, which is more representative of the tumor IM than Matrigel or bioengineered hydrogels, such as those prepared from polyethylene glycol (PEG) or alginate. These gaps are addressed, in part, by the present work.

Since modulation of the tumor ECM context and associated EMT are likely more of a continuum rather than a binary change [68], the influence of ECM composition and microstructure on tumor cell phenotypic transition was documented by varying IM:BM (Oligomer: Matrigel) ratio while maintaining a constant matrix stiffness. Interestingly, when three different PDAC lines were exposed separately to low-density Oligomer (100 Pa), they maintained their mesenchymal phenotype or showed evidence of EMT, with resultant morphology and protein expression profiles dependent upon initial cell line phenotype. On the other hand, Matrigel (100 Pa) inhibited EMT, promoted a clustered morphology for all cell types, and decreased mesenchymal protein expression. Such observations are consistent with the general expectation that IM is associated with mesenchymal behavior, and BM is involved in maintaining epithelial phenotype [66,67,69]. However, few *in-vitro* studies have demonstrated how simultaneous interaction of tumor cells with IM and BM contributes to EMT and phenotypic heterogeneity. Those studies that have done so, did not examine matrix microstructure and mechanics or compare different cell lines across the EMT spectrum [69,67,70].

In the present work, Matrigel induced epithelial BxPC-3 cells to grow as tight clusters, even when it was present in small amounts together with fibrillar type I collagen. Only in the 100:0 ratio, which had no Matrigel, did a subset of BxPC-3 undergo EMT, as indicated by a subpopulation of cells demonstrating spindle-shaped morphology, prominent vimentin staining, and some loss of E-cadherin staining. Population analysis by western blots supported the notion of matrix-induced EMT heterogeneity with little change in vimentin or E-cadherin expression and faint upregulation of fibronectin, another common marker for the mesenchymal phenotype. These findings for the epithelial PDAC line are consistent with a recent study where embedded normal mammary epithelial cells, MCF-10, only appeared invasive in monomeric type I collagen matrices [67]. When even small amounts of Matrigel were added to type I collagen matrices, MCF-10 displayed a more epithelial acinar phenotype.

On the other side of the EMT spectrum, MiaPaCa-2, which are classified as mesenchymal, showed more drastic morphological changes, as well as a decrease in mesenchymal protein expression as IM:BM ratio increased. An interesting observation was that combined IM and BM interactions in the 75:25 ratio appeared to promote a more invasive, elongated morphology than IM alone. Benton and colleagues reported similar findings with mesenchymal breast cancer cells, MDA-MB-231, which displayed the most invasive, migratory phenotypes when

Model	Schematic and Description	Cancer Type	Outcomes	Ref.
2D coatings (molecular)	 <ul style="list-style-type: none"> • Non-fibrillar • Type I collagen 	pancreatic	<ul style="list-style-type: none"> • Molecular type I collagen increases EMT via $\alpha_2\beta_1$ integrin mediated E-cadherin downregulation and vimentin upregulation 	[39,40,42]
3D single cell embedment	 <ul style="list-style-type: none"> • Fibrillar • Type I collagen 	pancreatic	<ul style="list-style-type: none"> • Type I collagen Oligomer promotes EMT of cells with Smad4 deletion • Matrigel promotes MET and hinders EMT • Interaction with collagen fibrils and BM components in Matrigel increases invasive phenotype of transitioned cells • Increasing fibril density decreases mesenchymal nature of cells 	Present work
		breast	<ul style="list-style-type: none"> • Type I collagen monomer matrices promotes invasive phenotype • Matrices with small amount of Matrigel promote acinar morphology 	[67]
	 <ul style="list-style-type: none"> • Non-fibrillar • PEG or alginate hydrogels 	pancreatic	<ul style="list-style-type: none"> • Exposure to TGF-β1 and EGF is necessary for EMT of cells grown in PEG hydrogels admixed with molecular type I collagen 	[79]
	breast	<ul style="list-style-type: none"> • Exposure to TGF-β1 is necessary for EMT of cells grown in RGD-alginate hydrogels; TGF-β1 removal results in EMT reversion (MET) 	[80]	
		breast, prostate, lung	<ul style="list-style-type: none"> • Incorporating GFOGER peptide ($\alpha_2\beta_1$ integrin binding sequence) into PEG hydrogels increases invasive phenotype 	[44]
Semi-3D (3D on top)	 <ul style="list-style-type: none"> • Fibrillar • Type I Collagen 	breast	<ul style="list-style-type: none"> • Larger fibril diameter leads to more spread, less clustered phenotype • Increasing fibril diameter and decreasing pore size increases invasiveness 	[43]
		breast	<ul style="list-style-type: none"> • Increasing fibril density of underlying collagen produces more proliferative, invasive phenotype 	[19]
		breast	<ul style="list-style-type: none"> • Type I collagen monomer matrices promotes mesenchymal phenotype • Matrices with laminin and collagen combined promote "invasive networks" of cells 	[69]
	 <ul style="list-style-type: none"> • Non-fibrillar • ECM-coated Polyacrylamide 	breast	<ul style="list-style-type: none"> • Increasing stiffness of type I collagen monomer- or Matrigel-coated polyacrylamide induces EMT 	[18]
	breast	<ul style="list-style-type: none"> • Increasing stiffness of Matrigel-coated polyacrylamide promotes a more invasive phenotype and loss of regular epithelial organization 	[19]	
		lung	<ul style="list-style-type: none"> • Increasing stiffness of fibronectin-coated substrates increases EMT • Inhibiting cell contractility abrogates this relationship suggesting cellular contractile machinery is necessary for EMT 	[73]
3D spheroid or organoid embedment		breast	<ul style="list-style-type: none"> • Increasing fibril density of type I collagen monomer matrices decreases tumor spheroid invasiveness 	[20]
	 <ul style="list-style-type: none"> • Fibrillar • Type I Collagen 	breast	<ul style="list-style-type: none"> • Maximum invasiveness and loss of epithelial organization occurs at intermediate density (stiffness) type I collagen monomer matrices 	[76]
		breast	<ul style="list-style-type: none"> • Maximum invasiveness occurs within a mixture of Matrigel and type I collagen 	[70]
		glioblastoma	<ul style="list-style-type: none"> • Maximum invasiveness occurs at intermediate stiffness of type I collagen Oligomer 	[22]
		breast	<ul style="list-style-type: none"> • Cells invading into a low fibril density matrix formed from type I collagen monomer were most sensitive to drug treatment and most invasive 	[21]
		breast	<ul style="list-style-type: none"> • Organoids show increased invasiveness and mesenchymal phenotype in type I collagen monomer matrices compared to Matrigel 	[66]

Note: EMT – Epithelial to mesenchymal transition; MET – Mesenchymal to epithelial transition; TGF- β 1 – Transforming growth factor β 1; EGF – Epidermal growth factor; PEG – Polyethylene glycol; RGD -- Arginine-Glycine-Aspartic acid

Fig 10. Models used to study role of ECM on EMT and invasion.

<https://doi.org/10.1371/journal.pone.0188870.g010>

cultured on-top or embedded as spheroids within matrices prepared from monomeric type I collagen and Matrigel [69,70]. Although the above-mentioned studies did not evaluate the matrix physical properties of IM-BM combinations, we noted that the 75:25 ratio was the only mixture of IM and BM that maintained the branched fibrillar architecture of type I collagen and the associated matrix stiffness (100 Pa). In summary, these observations suggest that for epithelial cells, Matrigel promotes epithelial morphogenesis regardless of the presence of an interconnected collagen fibrillar matrix, but for mesenchymal tumor cells, a stable, interconnected collagen fibrillar matrix with sufficient mechanical integrity is a primary factor in driving invasive phenotypes. These results also point to the need for further work to define how complex cell-ECM interactions such as those found at the tumor-stroma interface contribute to phenotypic heterogeneity and the continuum of EMT phenotypes observed *in vivo* [71].

Comparisons between our results and those in Fig 10 also revealed that the manner in which cells sense and respond to changes in substrate stiffness is highly dependent on the *in-vitro* model format (e.g., coated 2D, semi-3D, 3D embedded). Our results showed promotion of EMT and mesenchymal characteristics (e.g. spindle-shaped morphologies, vimentin and fibronectin expression) in PDAC cells embedded within relatively low-density collagen fibril matrices formed from Oligomer. When fibril density was increased, the resulting increased matrix stiffness and spatial constraints hindered mesenchymal-like cell spreading and resulted in confined, clustered growth. These results contradict observations from semi-3D models which have shown cells on-top of soft substrates maintained epithelial characteristics (clustered growth, E-cadherin expression, BM deposition) while increased substrate stiffness increased EMT-like behaviors including cell spreading, migration, and vimentin or fibronectin expression [18,19,72,73]. This trend was observed whether the underlying substrate on which cells were cultured was fibrillar type I collagen or non-fibrillar coatings of molecular type I collagen, Matrigel, or fibronectin on-top of PA gels. Therefore, the observed discrepancy between our results and those of semi-3D models is likely due to differences in geometric constraints. Specifically, the forced apical-basal polarization of cells imposed by semi-3D model geometry has been shown to alter the composition of cell-matrix adhesions and downstream signaling pathways in a manner different than 3D embedment models [74,75]. Assuming that EMT correlates with invasiveness, our results align more closely with those from 3D spheroid embedment models in which the most invasive phenotypes were observed in either the lowest or an intermediate stiffness type I collagen matrix while remaining more clustered at higher stiffness [20–22,76]. These 3D embedment models, including the present work, demonstrate that physical constraints experienced by cells within dense 3D matrices dominate over any increased signaling that may occur from increased ligand density or increased substrate stiffness as observed with semi-3D models. While some *in-vitro* studies aim to decouple matrix density and stiffness through non-natural matrix crosslinking [67,77], the relevance of these methods remains unclear since these two variables are naturally coupled with desmoplasia *in vivo* [56,77]. Taken together, these comparisons highlight that when developing accurate *in-vitro* tumor-ECM models, it is not just the presence of specific ECM ligands or “going 3D” that is important, but one must consider culture geometry, ligand presentation, and fibrillar architecture since all these features dictate EMT mechanobiology *in vivo*.

Our results also highlight two important, often overlooked aspects of 3D *in-vitro* models—the cell-matrix tension balance and the collagen fibril architecture [74,78]. In cancer, loss of cell-matrix tensional homeostasis and cell-induced alignment of type I collagen fibrils have been implicated in tumor progression and invasion [2,19]. Specifically, researchers have shown that increasing matrix tension by applying passive strain to monomeric type I collagen matrices increased invasiveness of embedded mammary organoids [76]. On the other hand, relieving intra-matrix tension by detaching similar collagen matrices from a culture dish

caused mammary epithelial cells to grow as tight acinar-like structures rather than the invasive, spindle-shaped morphologies observed in attached matrices [67]. In the present work, the high levels of Matrigel in low IM:BM ratios (50:50, 25:75) disrupted collagen fibril interconnectivity, which likely hindered cells ability to generate force and create tensional strain within the matrix. These mechanical changes, along with the BM signaling from Matrigel, are likely what caused clustered cell growth of both cell lines in these matrices. On the other hand, the type I collagen composition and interconnected fibril matrix of Oligomer (100:0) were sufficient to induce EMT of BxPC-3. Contrary to this result, non-fibrillar hydrogels such as collagen-PEG or RGD-alginate have been shown to not promote EMT in embedded pancreatic or breast cancer cells unless exogenous growth factors, such as TGF- β 1, were added [79,80]. It is important to note here that bioengineered materials such as those fashioned from alginate or PEG have no inherent bioactivity and lack physiologically relevant architecture. Even when molecular collagen (non-fibrillar) or RGD ligands are added to promote cell adhesion the architecture, mechanical properties, and resultant cell-substrate interactions that occur within these artificial microenvironments are dramatically different from those experienced by cells *in vivo*. From these observations, it is clear that *in-vitro* models of tumor EMT and invasion should be designed to accurately recreate ECM architectural features and cell-matrix mechanics for improved correlation between *in-vitro* and *in-vivo* behavior [2,74].

In addition to highlighting the importance of collagen fibril architecture in mechanistic study of tumor EMT and mechanobiology, observations from this work demonstrate the translational potential of Oligomer-based tumor-ECM models. Oligomer is unique among type I collagen formulations because of its purity, standardization, and ability for user customization, making it a powerful tool for creating standardized 3D models [23,25,30]. Additionally, its molecular make-up and its ability to form tissue-like collagen matrices with mature intermolecular crosslinks make Oligomer an ideal material for predicting *in-vivo* outcomes through recreating the ECM environment of desmoplastic tumors such as PDAC which are rich in type I collagen [3,24,25,53]. In fact, the observed trend in increased EMT behavior with decreased matrix density in the present work, has been recently noted in genetically engineered mouse models of PDAC [55,56]. In these studies, reduced stromal cell activity led to decreased desmoplasia and tumor stiffness which led to increased EMT, invasion and metastasis, as well as lower overall survival rates. The matrix-induced EMT heterogeneity in low-density Oligomer matrices is also reminiscent of observations from human clinical tumor samples in which only a subpopulation of cells undergoes EMT [71,81]. Finally, although only minor significant differences in drug sensitivity were found, this study demonstrates our ability to perform drug dosing experiments and generate IC50 values for these 3D tumor-ECM models. Collectively, these observations showcase the potential of Oligomer to serve as a robust platform for mechanistic study of metastasis and creation of predictive 3D drug screening models.

Conclusion

This work serves as a first step in the development of novel *in-vitro* 3D tumor-ECM models where Oligomer is used as a standardized type I collagen formulation to recreate and customize the IM component. From the foundational understanding of PDAC desmoplasia and EMT gained from these experiments, we can now develop more complex models of pancreatic and other cancers to systematically define the role of other prominent components of the tumor stromal microenvironment and study tumor invasion in more detail. Additionally, the model of matrix-driven EMT created by embedding PDAC cells within Oligomer-based fibril matrices provides a useful tool that can be applied to further mechanistic study. Finally, by developing and applying standardized *in-vitro* models with defined ECM microenvironments, we are

moving closer to accurately recreating tumor-stroma interactions and desmoplasia to provide pathophysiologically relevant PDAC models which can be used for phenotypic drug screening to ultimately predict therapeutic response and improve patient outcomes.

Supporting information

S1 Table. Comparison of gemcitabine IC50 values for PDAC lines cultured on 2D plastic. (DOCX)

Acknowledgments

The authors thank Sheng-Bin Peng and Shripad Bhagwat for their insight and editorial guidance in preparing this work for publication.

Author Contributions

Conceptualization: T. J. Puls, Catherine F. Whittington, Sherry L. Voytik-Harbin.

Data curation: T. J. Puls, Xiaohong Tan, Catherine F. Whittington.

Formal analysis: T. J. Puls, Xiaohong Tan, Catherine F. Whittington.

Funding acquisition: Sherry L. Voytik-Harbin.

Investigation: T. J. Puls, Xiaohong Tan, Catherine F. Whittington.

Methodology: T. J. Puls, Xiaohong Tan.

Project administration: T. J. Puls, Sherry L. Voytik-Harbin.

Resources: Sherry L. Voytik-Harbin.

Supervision: Sherry L. Voytik-Harbin.

Validation: T. J. Puls.

Visualization: T. J. Puls, Xiaohong Tan, Catherine F. Whittington.

Writing – original draft: T. J. Puls, Catherine F. Whittington, Sherry L. Voytik-Harbin.

Writing – review & editing: T. J. Puls, Catherine F. Whittington, Sherry L. Voytik-Harbin.

References

1. National Cancer Institute. Scientific Framework for Pancreatic Ductal Adenocarcinoma (PDAC). 2014.
2. Malik R, Lelkes PI, Cukierman E. Biomechanical and biochemical remodeling of stromal extracellular matrix in cancer. *Trends Biotechnol.* 2015; 33(4):230–6. <https://doi.org/10.1016/j.tibtech.2015.01.004> PMID: 25708906
3. Shields MA, Dangi-Garimella S, Redig AJ, Munshi HG. Biochemical role of the collagen-rich tumour microenvironment in pancreatic cancer progression. *Biochem J.* 2012 Jan 15; 441(2):541–52. <https://doi.org/10.1042/BJ20111240> PMID: 22187935
4. Pickup MW, Mouw JK, Weaver VM. The extracellular matrix modulates the hallmarks of cancer. *EMBO Rep.* 2014; 15(12):1243–53. <https://doi.org/10.15252/embr.201439246> PMID: 25381661
5. Gore J, Korc M. Pancreatic cancer stroma: friend or foe? *Cancer Cell.* 2014 Jun 16; 25(6):711–2. <https://doi.org/10.1016/j.ccr.2014.05.026> PMID: 24937454
6. Whatcott CJ, Posner RG, Von Hoff DD, Han H. Desmoplasia and chemoresistance in pancreatic cancer. In: Grippo PJ, Munshi HG, editors. *Pancreatic Cancer and Tumor Microenvironment*. India: Trans-world Research Network; 2012.
7. Erler JT, Weaver VM. Three-dimensional context regulation of metastasis. *Clin Exp Metastasis.* 2009; 26(1):35–49. <https://doi.org/10.1007/s10585-008-9209-8> PMID: 18814043

8. Zeisberg M, Neilson EG. Biomarkers for epithelial-mesenchymal transitions. *J Clin Invest.* 2009; 119(6):1429–37. <https://doi.org/10.1172/JCI36183> PMID: 19487819
9. Kalluri R, Weinberg RA. The basics of epithelial-mesenchymal transition. *J Clin Invest.* 2009; 119(6):1420–8. <https://doi.org/10.1172/JCI39104> PMID: 19487818
10. Klemm F, Joyce JA. Microenvironmental regulation of therapeutic response in cancer. *Trends Cell Biol.* 2015; 25(4):198–213. <https://doi.org/10.1016/j.tcb.2014.11.006> PMID: 25540894
11. Aclouque H, Adams MS, Fishwick K, Bronner-Fraser M, Nieto MA. Epithelial-mesenchymal transitions: The importance of changing cell state in development and disease. *J Clin Invest.* 2009; 119(6):1438–49. <https://doi.org/10.1172/JCI38019> PMID: 19487820
12. O'Connor JW, Gomez EW. Biomechanics of TGFβ-induced epithelial-mesenchymal transition: implications for fibrosis and cancer. *Clin Transl Med.* 2014; 3(23).
13. Wei SC, Fattet L, Yang J. The forces behind EMT and tumor metastasis. *Cell Cycle.* 2015; 14(15):2387–8. <https://doi.org/10.1080/15384101.2015.1063296> PMID: 26083471
14. Craene B De, Bex G. Regulatory networks defining EMT during cancer initiation and progression. *Nat Rev Cancer.* 2013; 13(2):97–110. <https://doi.org/10.1038/nrc3447> PMID: 23344542
15. Lamouille S, Xu J, Derynck R. Molecular mechanisms of epithelial-mesenchymal transition. *Nat Rev Mol Cell Biol.* 2014 Mar; 15(3):178–96. <https://doi.org/10.1038/nrm3758> PMID: 24556840
16. Kimlin LC, Casagrande G, Virador VM. In vitro three-dimensional (3D) models in cancer research: an update. *Mol Carcinog.* 2013 Mar; 52(3):167–82. <https://doi.org/10.1002/mc.21844> PMID: 22162252
17. Yamada KM, Cukierman E. Modeling tissue morphogenesis and cancer in 3D. *Cell.* 2007 Aug 24; 130(4):601–10. <https://doi.org/10.1016/j.cell.2007.08.006> PMID: 17719539
18. Wei SC, Fattet L, Tsai JH, Guo Y, Pai VH, Majeski HE, et al. Matrix stiffness drives epithelial-mesenchymal transition and tumour metastasis through a TWIST1–G3BP2 mechanotransduction pathway. *Nat Cell Biol.* 2015; 17(5):678–688. <https://doi.org/10.1038/ncb3157> PMID: 25893917
19. Paszek MJ, Zahir N, Johnson KR, Lakins JN, Rozenberg GI, Gefen A, et al. Tensional homeostasis and the malignant phenotype. *Cancer Cell.* 2005 Sep; 8(3):241–54. <https://doi.org/10.1016/j.ccr.2005.08.010> PMID: 16169468
20. Guzman A, Ziperstein MJ, Kaufman LJ. The effect of fibrillar matrix architecture on tumor cell invasion of physically challenging environments. *Biomaterials.* 2014; 35(25):6954–63. <https://doi.org/10.1016/j.biomaterials.2014.04.086> PMID: 24835043
21. Lam RCI, Wong HK, Nai S, Chua CK, Tan NS, Tan LP. A 3D Biomimetic Model of Tissue Stiffness Interface for Cancer Drug Testing. *Mol Pharm.* 2014; 11:2016–21. <https://doi.org/10.1021/mp500059q> PMID: 24754837
22. Herrera-Perez M, Voytik-Harbin S, Rickus JL. Extracellular matrix properties regulate the migratory response of glioblastoma stem cells in 3D culture. *Tissue Eng Part A.* 2015; 21:2572–82. <https://doi.org/10.1089/ten.TEA.2014.0504> PMID: 26161688
23. Kreger ST, Bell BJ, Bailey J, Stites E, Kuske J, Waisner B, et al. Polymerization and matrix physical properties as important design considerations for soluble collagen formulations. *Biopolymers.* 2010 Aug; 93(8):690–707. <https://doi.org/10.1002/bip.21431> PMID: 20235198
24. Blum KM, Novak T, Watkins L, Neu CP, Wallace JM, Bart ZR, et al. Acellular and cellular high-density, collagen-fibril constructs with suprafibrillar organization. *Biomater Sci.* 2016; 4(4):711–23. <https://doi.org/10.1039/c5bm00443h> PMID: 26902645
25. Bailey JL, Critser PJ, Whittington C, Kuske JL, Yoder MC, Voytik-Harbin SL. Collagen oligomers modulate physical and biological properties of three-dimensional self-assembled matrices. *Biopolymers.* 2011 Feb; 95(2):77–93. <https://doi.org/10.1002/bip.21537> PMID: 20740490
26. Whittington CF, Yoder MC, Voytik-Harbin SL. Collagen-polymer guidance of vessel network formation and stabilization by endothelial colony forming cells in vitro. *Macromol Biosci.* 2013 Jul 5; 1–15.
27. Monteleon CL, Sedgwick A, Hartsell A, Dai M, Whittington C, Voytik-Harbin S, et al. Establishing epithelial glandular polarity: interlinked roles for ARF6, Rac1, and the matrix microenvironment. *Mol Biol Cell.* 2012 Dec; 23(23):4495–505. <https://doi.org/10.1091/mbc.E12-03-0246> PMID: 23051733
28. Benton G, Arnaoutova I, George J, Kleinman HK, Koblinski J. Matrigel: From discovery and ECM mimicry to assays and models for cancer research. *Adv Drug Deliv Rev.* 2014 Jul 2; 79–80:3–8. <https://doi.org/10.1016/j.addr.2014.06.005> PMID: 24997339
29. Johnson KR, Leight JL, Weaver VM. Demystifying the Effects of a Three-Dimensional Microenvironment in Tissue Morphogenesis. *Methods Cell Biol.* 2007; 83:547–83. [https://doi.org/10.1016/S0091-679X\(07\)83023-8](https://doi.org/10.1016/S0091-679X(07)83023-8) PMID: 17613324
30. ASTM International. ASTM Standard F3089: Standard Guide for Characterization and Standardization of Polymerizable Collagen-based Products and Associated Collagen-cell Interactions. West Conshohocken, PA; 2014.

31. Weigelt B, Ghajar CM, Bissell MJ. The need for complex 3D culture models to unravel novel pathways and identify accurate biomarkers in breast cancer. *Adv Drug Deliv Rev.* 2014; 69–70:42–51. <https://doi.org/10.1016/j.addr.2014.01.001> PMID: 24412474
32. Whittington C, Brandner E. Oligomers Modulate Interfibril Branching and Mass Transport Properties of Collagen Matrices. *Microsc* 2013; 19(5):1323–33.
33. Brightman AO, Rajwa BP, Sturgis JE, McCallister ME, Robinson JP, Voytik-Harbin SL. Time-lapse confocal reflection microscopy of collagen fibrillogenesis and extracellular matrix assembly in vitro. *Biopolymers.* 2000 Sep; 54(3):222–34. [https://doi.org/10.1002/1097-0282\(200009\)54:3<222::AID-BIP80>3.0.CO;2-K](https://doi.org/10.1002/1097-0282(200009)54:3<222::AID-BIP80>3.0.CO;2-K) PMID: 10861383
34. Kokkinos MI, Wafai R, Wong MK, Newgreen DF, Thompson EW, Waltham M. Vimentin and epithelial-mesenchymal transition in human breast cancer—Observations in vitro and in vivo. *Cells Tissues Organs.* 2007; 185(1–3):191–203. <https://doi.org/10.1159/000101320> PMID: 17587825
35. Morris HT, Machesky LM. Actin cytoskeletal control during epithelial to mesenchymal transition: focus on the pancreas and intestinal tract. *Br J Cancer.* 2015; 112(4):613–20. <https://doi.org/10.1038/bjc.2014.658> PMID: 25611303
36. Deer EL, Gonzalez-Hernandez J, Coursen JD, Shea JE, Ngatia J, Scaife CL, et al. Phenotype and Genotype of Pancreatic Cancer Cell Lines. *Pancreas.* 2010; 39(4):425–35. <https://doi.org/10.1097/MPA.0b013e3181c15963> PMID: 20418756
37. Teixidó C, Marés R, Aracil M, Ramón y Cajal S, Hernández-Losa J. Epithelial-mesenchymal transition markers and HER3 expression are predictors of elisidepsin treatment response in breast and pancreatic cancer cell lines. *PLoS One.* 2013 Jan; 8(1):e53645. <https://doi.org/10.1371/journal.pone.0053645> PMID: 23320098
38. Arumugam T, Ramachandran V, Fournier KF, Wang H, Marquis L, Abbruzzese JL, et al. Epithelial to mesenchymal transition contributes to drug resistance in pancreatic cancer. *Cancer Res.* 2009 Jul 15; 69(14):5820–8. <https://doi.org/10.1158/0008-5472.CAN-08-2819> PMID: 19584296
39. Menke A, Philippi C, Vogelmann R, Seidel B, Lutz MP, Adler G, et al. Down-Regulation of E-Cadherin Gene Expression by Collagen Type I and Type III in Pancreatic Cancer Cell Lines 1. *Cancer Res.* 2001; 61:3508–17. PMID: 11309315
40. Medici D, Nawshad A. Type I collagen promotes epithelial-mesenchymal transition through ILK-dependent activation of NF- κ B and LEF-1. *Matrix Biol.* 2009; 29(3):161–5. <https://doi.org/10.1016/j.matbio.2009.12.003> PMID: 20018240
41. Walsh LA, Nawshad A, Medici D. Discoidin domain receptor 2 is a critical regulator of epithelial-mesenchymal transition. *Matrix Biol.* 2011; 30(4):243–7. <https://doi.org/10.1016/j.matbio.2011.03.007> PMID: 21477649
42. Koenig A, Mueller C, Hasel C, Adler G, Menke A. Collagen type I induces disruption of E-cadherin-mediated cell-cell contacts and promotes proliferation of pancreatic carcinoma cells. *Cancer Res.* 2006; 66(9):4662–71. <https://doi.org/10.1158/0008-5472.CAN-05-2804> PMID: 16651417
43. Sapudom J, Rubner S, Martin S, Kurth T, Riedel S, Mierke CT, et al. The phenotype of cancer cell invasion controlled by fibril diameter and pore size of 3D collagen networks. *Biomaterials.* 2015; 52:367–75. <https://doi.org/10.1016/j.biomaterials.2015.02.022> PMID: 25818443
44. Taubenberger A V., Bray LJ, Haller B, Shaposhnykov A, Binner M, Freudenberg U, et al. 3D extracellular matrix interactions modulate tumour cell growth, invasion and angiogenesis in engineered tumour microenvironments. *Acta Biomater.* 2016; 36:73–85. <https://doi.org/10.1016/j.actbio.2016.03.017> PMID: 26971667
45. Breslin S, O'Driscoll L. Three-dimensional cell culture: the missing link in drug discovery. *Drug Discov Today.* 2013 Mar; 18(5–6):240–9. <https://doi.org/10.1016/j.drudis.2012.10.003> PMID: 23073387
46. Lee DW, Choi Y, Seo YJ, Lee M, Jeon SY, Ku B. High-Throughput Screening (HTS) of Anticancer Drug Efficacy on a Micropillar/Microwell Chip Platform. *Anal Chem.* 2014; 86:535–42. <https://doi.org/10.1021/ac402546b> PMID: 24199994
47. Seguin L, Desgrosellier JS, Weis SM, Cheresh DA. Integrins and cancer: regulators of cancer stemness, metastasis, and drug resistance. *Trends Cell Biol.* 2015; 25(4):234–40. <https://doi.org/10.1016/j.tcb.2014.12.006> PMID: 25572304
48. Multhaupt HAB, Leitinger B, Gullberg D, Couchman JR. Extracellular matrix component signaling in cancer. *Adv Drug Deliv Rev.* 2016; 97:28–40. <https://doi.org/10.1016/j.addr.2015.10.013> PMID: 26519775
49. Armstrong T, Packham G, Murphy LB, Bateman AC, Conti JA, Fine DR, et al. Type I Collagen Promotes the Malignant Phenotype of Pancreatic Ductal Adenocarcinoma. *Clin Cancer Res.* 2004; 10:7427–37. <https://doi.org/10.1158/1078-0432.CCR-03-0825> PMID: 15534120

50. Feig C, Gopinathan A, Neesse A, Chan DS, Cook N, Tuveson DA. The pancreas cancer microenvironment. *Clin Cancer Res.* 2012; 18(16):4266–76. <https://doi.org/10.1158/1078-0432.CCR-11-3114> PMID: 22896693
51. Tang D, Wang D, Yuan Z, Xue X, Zhang Y, An Y, et al. Persistent activation of pancreatic stellate cells creates a microenvironment favorable for the malignant behavior of pancreatic ductal adenocarcinoma. *Int J Cancer.* 2013; 132(5):993–1003. <https://doi.org/10.1002/ijc.27715> PMID: 22777597
52. Hamed SS, Straubinger RM, Jusko WJ. Pharmacodynamic modeling of cell cycle and apoptotic effects of gemcitabine on pancreatic adenocarcinoma cells. *Cancer Chemother Pharmacol.* 2013; 72(3):553–63. <https://doi.org/10.1007/s00280-013-2226-6> PMID: 23835677
53. Whatcott CJ, Diep CH, Jiang P, Watanabe A, Lobello J, Sima C, et al. Desmoplasia in primary tumors and metastatic lesions of pancreatic cancer. *Clin Cancer Res.* 2015; 21(15):3561–8. <https://doi.org/10.1158/1078-0432.CCR-14-1051> PMID: 25695692
54. Han B, Qu C, Park K, Konieczny SF, Korc M. Recapitulation of complex transport and action of drugs at the tumor microenvironment using tumor-microenvironment-on-chip. *Cancer Lett.* 2016; 380:319–29. <https://doi.org/10.1016/j.canlet.2015.12.003> PMID: 26688098
55. Rhim AD, Oberstein PE, Thomas DH, Mirek ET, Palermo CF, Sastra SA, et al. Stromal Elements Act to Restrain, Rather Than Support, Pancreatic Ductal Adenocarcinoma. *Cancer Cell.* 2014; 25(6):735–47. <https://doi.org/10.1016/j.ccr.2014.04.021> PMID: 24856585
56. Ozdemir BC, Pentcheva-Hoang T, Carstens JL, Zheng X, Wu CC, Simpson TR, et al. Depletion of carcinoma-associated fibroblasts and fibrosis induces immunosuppression and accelerates pancreas cancer with reduced survival. *Cancer Cell.* 2014; 25(6):719–34. <https://doi.org/10.1016/j.ccr.2014.04.005> PMID: 24856586
57. Rowe RG, Weiss SJ. Breaching the basement membrane: who, when and how? *Trends Cell Biol.* 2008; 18(11):560–74. <https://doi.org/10.1016/j.tcb.2008.08.007> PMID: 18848450
58. Rowe RG, Weiss SJ. Navigating ECM barriers at the invasive front: the cancer cell-stroma interface. *Annu Rev Cell Dev Biol.* 2009; 25:567–95. <https://doi.org/10.1146/annurev.cellbio.24.110707.175315> PMID: 19575644
59. Birk DE, Bruckner P. Collagens, Suprastructures, and Collagen Fibril Assembly. In: Mecham RP, editor. *The Extracellular Matrix: an Overview.* Berlin, Heidelberg: Springer-Verlag; 2011. p. 77–115.
60. Eyre DR, Wu J-J. Collagen Cross-Links. Brinckman J, Notbohm H, Muller PK, editors. *Top Curr Chem.* 2005; 247:207–29.
61. Van Der Zee JA, Van Eijck CH, Hop WC, Biermann K, Dicheva BM, Seynhaeve AL, et al. Tumour basement membrane laminin expression predicts outcome following curative resection of pancreatic head cancer. *Br J Cancer.* 2012; 107(7):1153–8. <https://doi.org/10.1038/bjc.2012.373> PMID: 22929879
62. Benton G, Kleinman HK, George J, Arnaoutova I. Multiple uses of basement membrane-like matrix (BME/Matrigel) in vitro and in vivo with cancer cells. *Int J Cancer.* 2011; 128(8):1751–7. <https://doi.org/10.1002/ijc.25781> PMID: 21344372
63. Brookes S, Voytik-harbin S, Zhang H, Halum S. 3-Dimensional (3D) Tissue-Engineered Skeletal Muscle for Laryngeal Reconstruction. *Laryngoscope.* 2017;
64. Cukierman E, Pankov R, Yamada KM. Cell interactions with three-dimensional matrices. *Curr Opin Cell Biol.* 2002; 14(5):633–9. PMID: 12231360
65. Katz E, Dubois-Marshall S, Sims AH, Gautier P, Caldwell H, Meehan RR, et al. An In Vitro model that recapitulates the epithelial to Mesenchymal transition (EMT) in Human Breast Cancer. *PLoS One.* 2011; 6(2).
66. Nguyen-Ngoc K-V, Cheung KJ, Brenot A, Shamir ER, Gray RS, Hines WC, et al. ECM microenvironment regulates collective migration and local dissemination in normal and malignant mammary epithelium. *Proc Natl Acad Sci.* 2012; 109(39):E2595–604. <https://doi.org/10.1073/pnas.1212834109> PMID: 22923691
67. Carey SP, Martin KE, Reinhart-king CA. Three-dimensional collagen matrix induces a mechanosensitive invasive epithelial phenotype. *Sci Rep.* 2017; 7(42088).
68. Mandal M, Ghosh B, Anura A, Mitra P, Pathak T, Chatterjee J. Modeling continuum of epithelial mesenchymal transition plasticity. *Integr Biol.* 2016; 8:167–76.
69. Benton G, Crooke E, George J. Laminin-1 induces E-cadherin expression in 3-dimensional cultured breast cancer cells by inhibiting DNA methyltransferase 1 and reversing promoter methylation status. *FASEB J.* 2009; 23(11):3884–95. <https://doi.org/10.1096/fj.08-128702> PMID: 19635753
70. Benton G, DeGray G, Kleinman HK, George J, Arnaoutova I. In Vitro Microtumors Provide a Physiologically Predictive Tool for Breast Cancer Therapeutic Screening. *PLoS One.* 2015; 10:e0123312. <https://doi.org/10.1371/journal.pone.0123312> PMID: 25856378

71. Klymkowsky MW, Savagner P. Epithelial-Mesenchymal Transition: A Cancer Researcher's Conceptual Friend and Foe. *Am J Pathol.* 2009; 174(5):1588–93. <https://doi.org/10.2353/ajpath.2009.080545> PMID: 19342369
72. Tilghman RW, Cowan CR, Mih JD, Koryakina Y, Gioeli D, Slack-Davis JK, et al. Matrix rigidity regulates cancer cell growth and cellular phenotype. *PLoS One.* 2010; 5(9):1–13.
73. Markowski MC, Brown AC, Barker TH. Directing epithelial to mesenchymal transition through engineered microenvironments displaying orthogonal adhesive and mechanical cues. *J Biomed Mater Res—Part A.* 2012; 100 A(8):2119–27.
74. Harunaga JS, Yamada KM. Cell-matrix adhesions in 3D. *Matrix Biol.* 2011; 30(7–8):363–8. <https://doi.org/10.1016/j.matbio.2011.06.001> PMID: 21723391
75. Pathak A, Kumar S. Biophysical regulation of tumor cell invasion: moving beyond matrix stiffness. *Integr Biol.* 2011; 3:267–78.
76. Cassereau L, Miroshnikova YA, Ou G, Lakins J, Weaver VM. A 3D tension bioreactor platform to study the interplay between ECM stiffness and tumor phenotype. *J Biotechnol.* 2015; 193:66–9. <https://doi.org/10.1016/j.jbiotec.2014.11.008> PMID: 25435379
77. Levental KR, Yu H, Kass L, Lakins JN, Egeblad M, Erler JT, et al. Matrix crosslinking forces tumor progression by enhancing integrin signaling. *Cell.* 2009 Nov 25; 139(5):891–906. <https://doi.org/10.1016/j.cell.2009.10.027> PMID: 19931152
78. Egeblad M, Rasch MG, Weaver VM. Dynamic interplay between the collagen scaffold and tumor evolution. *Curr Opin Cell Biol.* 2010; 22(5):697–706. <https://doi.org/10.1016/j.ceb.2010.08.015> PMID: 20822891
79. Ki CS, Lin T-Y, Korc M, Lin C-C. Thiol-ene hydrogels as desmoplasia-mimetic matrices for modeling pancreatic cancer cell growth, invasion, and drug resistance. *Biomaterials.* 2014 Dec; 35(36):9668–77. <https://doi.org/10.1016/j.biomaterials.2014.08.014> PMID: 25176061
80. Bidarra SJ, Oliveira P, Rocha S, Saraiva DP, Oliveira C, Barrias CC. A 3D in vitro model to explore the inter-conversion between epithelial and mesenchymal states during EMT and its reversion. *Sci Rep.* 2016; 6(February):27072. <https://doi.org/10.1038/srep27072> PMID: 27255191
81. Creighton CJ, Gibbons DL, Kurie JM. The role of epithelial-mesenchymal transition programming in invasion and metastasis: A clinical perspective. *Cancer Manag Res.* 2013; 5(1):187–95.